

Summer 2022

Sex Differences and Potential Non-invasive Treatments for Calcific Aortic Valve Disease

Henry Pascal Helms

Follow this and additional works at: <https://scholarcommons.sc.edu/etd>



Part of the [Biomedical Commons](#)

Recommended Citation

Helms, H. P.(2022). *Sex Differences and Potential Non-invasive Treatments for Calcific Aortic Valve Disease*. (Master's thesis). Retrieved from <https://scholarcommons.sc.edu/etd/6895>

This Open Access Thesis is brought to you by Scholar Commons. It has been accepted for inclusion in Theses and Dissertations by an authorized administrator of Scholar Commons. For more information, please contact digres@mailbox.sc.edu.

SEX DIFFERENCES AND POTENTIAL NON-INVASIVE TREATMENTS FOR
CALCIFIC AORTIC VALVE DISEASE

by

Henry Pascal Helms

Bachelor of Science
University of South Carolina, 2019

Submitted in Partial Fulfillment of the Requirements

For the Degree of Master of Science in

Biomedical Science

School of Medicine-Columbia

University of South Carolina

2022

Accepted by:

Mohamad Azhar, Director of Thesis

Holly LaVoie, Reader

Reilly Enos, Reader

Tracey L. Weldon, Vice Provost and Dean of the Graduate School

© Copyright by Henry Paschal Helms, 2022
All Rights Reserved.

DEDICATION

I would like to dedicate my thesis to my family. Mom and Dad, I am beyond blessed to have your guidance, support, and love. To my brother and sister, thank you for being two of my dearest friends. All of you bring light to my life with love and laughter.

ACKNOWLEDGMENTS

I will start by thanking Dr. Azhar for giving me the opportunity to work in his lab. I could not ask for a better mentor. His knowledge and passion for research motivated me to perform at my best. I would like to thank Dr. Mrinmay Chakrabarti and PhD student Mengistu Gebere for being good friends and mentors in the lab. They selflessly took time out of their busy schedules to train me and help me whenever it was needed. I would also like to thank Danielle Prissendorf for assisting with echocardiograms. Not all of them turned out as well as one may like, but your company was much appreciated during the early sessions of that venture. I also need to thank fellow Master student Hannah Ji for helping with various tasks around the lab such as microCT scans.

I would like to thank Dr. Edie Goldsmith for providing me with the opportunity to be a part of the Integrated Biomedical Sciences program and providing guidance when I decided I wanted to leave the program. I also want to thank Joann Nagy for all of her help. She's one of the most compassionate people I have met. She always kept in touch to make sure I was on track with school and classes (things that would've otherwise slipped my mind), and we shared many wonderful conversations over the past couple of years.

I would like to thank a couple of my previous mentors here at the medical school, Dr. Kandy Velazquez and Dr. Ana Pocivavsek. Kandy's lab was the first place I got research experience, and I spent several great months there before COVID shut things down. I will forever carry a unique expertise in judging the health of mouse poop due to my time there. My time in Dr. Pocivavsek's lab was very impactful on the course of my

life. It was there that I faced a crossroad in my life. I had a long conversation with post doc, Snezana Milosavljevic, one evening, and decided that I had to resume my pursuit of becoming a physician. It's cheesy and cliché, but I had to follow my dreams. Thanks to all of you. You've all been a wonderful part of my life.

ABSTRACT

Calcific Aortic Valve Disease (CAVD) is a progressive heart disease that ranges from aortic valve sclerosis to aortic valve stenosis. It is characterized by intense calcification and compromised valve function. CAVD affects 25% of people older than 65 and 50% of people older than 85. These rates are expected to increase in the United States due to higher levels of obesity and diabetes, as well as an aging population. CAVD is the leading cause of valve replacement surgery. Annual healthcare costs for these valve replacements are currently estimated to be approximately 2 billion dollars. There are currently no medications approved by the FDA to treat CAVD.

This thesis focuses on two potential pathways to non-invasively treat CAVD. First, male sex is widely considered to be a major risk factor. The goal of one project is to understand why this is, as insights at the molecular level could lead to the treatment of CAVD using medication or supplements such as estrogen supplements. The results suggest that estrogen is protective in female VICs, but this is not the case for male VICs.

The second project centers on studying whether targeted EDTA chelation therapy (via nanoparticles) can reduce calcification of the aortic valve and improve heart function. The results indicate that this method is capable of reducing calcification in the aortic valve.

TABLE OF CONTENTS

Dedication	iii
Acknowledgements	iv
Abstract	vi
List of Tables	viii
List of Figures	ix
List of Symbols	xi
List of Abbreviations	xii
Chapter 1 BACKGROUND ON CALCIFIC AORTIC VALVE DISEASE.....	1
Chapter 2 THE IMPACT OF SEX HORMONES IN CALCIFIC AORTIC VALVE DISEASE	15
Chapter 3 THE POTENTIAL OF EDTA AS A NON-INVASIVE TREATMENT OF CALCIFIC AORTIC VALVE DISEASE	51
References.....	71
Appendix A: Additional Figures.....	84

LIST OF TABLES

Table 2.1 Genetic Background of Mice	37
--	----

LIST OF FIGURES

Figure 1.1 Anatomy of the Aorta.....	9
Figure 1.2 Diagram of Aortic Leaflets.....	10
Figure 1.3 Cross Section of AV Leaflet.....	11
Figure 1.4 Progression of CAVD.....	12
Figure 1.5 Structure of TGF β 1	13
Figure 1.6 TGF β 1 Signaling Pathway	14
Figure 2.1 Estrogen and Androgen Signaling.....	35
Figure 2.2 Diagram of TGF β 1 Transgenic Mice Genetic Model	36
Figure 2.3 Quantification of Calcification via mCT Imaging of Preliminary OVX Study.....	38
Figure 2.4 Alizarin Red Staining of the AVs of Preliminary OVX Study	39
Figure 2.5 mCT Imaging of Each Mouse in Preliminary OVX Study	40
Figure 2.6 Doppler Imaging of AV from Preliminary OVX Study.....	41
Figure 2.7 Changes in Peak AV Pressure of Mice in Preliminary OVX Study.....	42
Figure 2.8 Quantification of Calcification of Female Murine VICs in Cell Culture.....	43
Figure 2.9 Representative Images of Wells in Female Cell Cultures	44
Figure 2.10 Quantification of Calcification of Male Murine VICs in Cell Culture	45
Figure 2.11 Representative Images of Wells in Male Cell Cultures.....	46
Figure 2.12 Alizarin Red Staining of AV from OVX & CAST Study.....	47

Figure 2.13 Quantification of Calcification and Volume Nodule in OVX & CAST Study	48
Figure 2.14 Doppler Imaging from OVX & CAST Project.....	49
Figure 2.15 Initial and Final Peak AV Pressure in OVX & CAST Study	50
Figure 3.1 Structure of Albumin Nanoparticle	64
Figure 3.2 Comparison of Healthy vs Damaged Elastin Fibers.....	65
Figure 3.3 Histological Staining of Aortic Valve After Targeted EDTA Treatment.	66
Figure 3.4 microCT of Aortic Valve Before and After Targeted EDTA Treatment	67
Figure 3.5 Quantification of Reduced Calcification.....	68
Figure 3.6 Reduction in Volume of Calcific Nodule.....	69
Figure 3.7 Impact of EDTA on Left Ventricular Function.....	70
Figure A. 1 Weights of Mice in Preliminary OVX Study	84
Figure A. 2 Weights of Mice in OVX and CAST Study	85
Figure A. 3 qPCR Comparison of ER α Expression in AV of Mice	86

LIST OF SYMBOLS

°C Degrees Celsius

AU Arbitrary Units

mg Milligram

mm Millimeter

kg Kilogram

mmHg Millimeter of mercury

LIST OF ABBREVIATIONS

AAV	Aortic Arch View
AR	Androgen Receptor
AoR	Aortic Root
AV	Aortic Valve
BMP	Bone Morphogenetic Protein
CAST	Castration
CAVD	Calcific Aortic Valve Disease
DHT	Dihydrotestosterone
DMEM	Dulbecco's Modified Eagle Medium
DMSO	Dimethyl sulfoxide
dTg	Double Transgenic
E	Estradiol
EDTA	Ethylenediaminetetraacetic Acid
EMT	Endothelial-to-Mesenchymal Transition
EBP	Estrogen Binding Protein
ER α	Estrogen Receptor alpha
ER β	Estrogen Receptor beta
FBS	Fetal Bovine Serum
HFD	High Fat Diet
HEPES	4-(2-hydroxyethyl)-1-piperazineethanesulfonic acid

LV	Left Ventricle
mCT	microCT
NP	Nanoparticle
nTg	Non-transgenic
mT/mG ..	membrane-targeted tandem dimer Tomato/membrane-targeted green fluorescent protein
OTC.....	Optimal cutting temperature
OST	Osteogenic
PBS	Phosphate Buffer Saline
PLAX	Parasternal Long Axis
PSAX	Parasternal Short Axis
Runx2.....	Runt-related transcription factor 2
Smad	Mothers Against Decapentaplegic Homolog
Tg	Transgenic
TGF β	Transforming Growth Factor Beta
TGF β 1	Transforming Growth Factor Beta 1
TGF β 1-3.....	Transforming Growth Factor Beta 1, 2, and 3
T β RI	TGF β receptor type I
T β RII.....	TGF β receptor type II
VECs.....	Valve Endothelial Cells
VICs	Valve Interstitial Cells

CHAPTER 1

BACKGROUND ON CALCIFIC AORTIC VALVE DISEASE

1.1 Structure, Function, and Histology of the Aortic Valve

The aortic root (AoR) (Figure 1.1) is a centrally located structure in the heart that runs from the output of the left ventricle to the point where the output joins with the ascending aorta (Ho, 2009). The AoR is where oxygenated blood moves from the heart to the aorta and then into systemic circulation of the body (Weinhaus, 2015). The AoR is composed of several structures: the annulus, commissures, interleaflet triangles, sinus of Valsalva, sinutubular junction, and leaflets (Misfeld and Sievers, 2007). The aortic valve (AV) is located within the AoR and is composed of three leaflets that form a hemodynamic, physical border between the left ventricle (LV) and aorta (Charitos & Sievers, 2013). The three leaflets are the left coronary leaflet, the right coronary leaflet, and the non-coronary leaflet (Figure 1.2) (Ho, 2009). The left and right coronary leaflets earned their name by being located adjacent to the left and right coronary artery, respectively, while the non-coronary leaflet is not located adjacent to either coronary artery (Charitos & Sievers, 2013).

Blood moves from the LV to the aorta through the AV when pressure in the LV exceeds that of the AoR which pushes the leaflets open, allowing blood to flow through (systole) (Charitos & Sievers, 2013). When the pressure of the aorta exceeds that of the LV, then the leaflets are forced back into the closed position (diastole). It is critical

for the AV to have the three leaflet design. It is the optimal formation for low resistance opening of the valve, as evidenced by people who have bicuspid aortic valves and suffer from valve dysfunction or stenosis associated with it (Thubrikar, 1981; Sievers & Schmidtke, 2007).

These collagenous leaflets are composed of four parts: the belly, the hinge, the coapting surface and the lannula with the noduli of Arantii (Misfeld & Sievers, 2007). The hinge is the where the leaflets attach to the crescent-shaped annulus of the AoR, and it absorbs the stress experienced by the leaflets during blood flow and directs it to the aortic wall (Misfeld & Sievers, 2007). The belly is the main part of the leaflet. This portion is semi-translucent, which has made it easy to study its highly structured arrangement of collagen (Misfeld & Sievers, 2007). Valve endothelial cells (VECs) line the outer portions of the leaflets, and the interior of the structure is primarily filled out with valve interstitial cells (VICs) (Misfeld & Sievers, 2007). Other cells such as haemopoietic-derived stem cells, myofibroblasts, and smooth muscle cells are also present (Taylor et al., 2003; Visconti et al., 2006). The interior of the leaflets are divided into three primary layers: lamina fibrosa, lamina spongiosa, and lamina ventricularis (Figure 1.3) (Misfeld & Sievers, 2007). The three layers have different compositions of matrix, but they are all populated by VICs. These VICs originate from endothelial cells that move into the matrix during embryogenesis and undergo endothelial-to-mesenchymal transition (EMT) (Butcher & Markwald, 2007).

VICs are designated as fibroblast-like cells that are responsible for secreting and preserving the extracellular matrix of the leaflets (Chen et al., 2009; Rutkovskiy et al., 2017). Environmental and molecular changes can cause VICs to differentiate into

osteoblasts, adipocytes and chondrocytes or to be activated as myofibroblasts (Chen et al., 2009; Rutkovskiy et al., 2017). Myofibroblasts display characteristics of fibroblasts and smooth muscle cells (Messier et al., 1994; Filip et al., 1986). They are fibroblasts that, like smooth muscle cells, possess the ability to contract (Rutkovskiy et al., 2017). Aortic VICs from pigs have better contractability in their extracellular matrix compared to pulmonary VICs (Merryman et al., 2007).

1.2 Calcific Aortic Valve Disease (CAVD)

Calcific Aortic Valve Disease (CAVD) is the third most common cardiovascular disease and the leading cause of valve disease in the developed world (Iung et al., 2003; Rutkovskiy et al., 2017). Metabolic syndrome, male sex, obesity, diabetes, high circulating lipid levels, and smoking are some of the most common risk factors associated with CAVD (O'Brien, 2007; Yutzey et al., 2014). Disease burden of CAVD is projected to increase from 2.5 million cases in 2000 to 4.5 million cases by 2030 (Aikawa & Schoen, 2014). Changes in the cells of the aortic leaflets accumulate, leading to aortic sclerosis and, eventually, aortic stenosis (Figure 1.4) (Rajamannan et al., 2011). As CAVD progresses from aortic sclerosis to stenosis, valvular function is hindered which results in angina, left ventricular hypertrophy, heart failure, and death (Rajamannan et al., 2011; Yutzey et al., 2014).

An effective non-invasive treatment has yet to be developed (Yutzey et al., 2014). The only way to assist a patient with CAVD is through aortic valve replacement either with a transcatheter or bioprosthetic valve (Nishimura et al., 2014). Valve replacement is costly, risky to the patient, and, in the case of bioprosthetic replacement, requires repeat surgery later (Rajamannan et al., 2011; Linman et al., 2013). The

bioprosthetic replacements calcify within 10 to 15 years, and patients that receive a transcatheter installation require anticoagulation treatments for the rest of their lives (Rutkovskiy et al., 2017). Our understanding of the disease is expanding, and there is hope for the development of non-invasive treatments.

It appears that, over time, passive degradation of the leaflets gives way to the active changes that occur at the cellular and molecular level that lead to deposition of calcium. CAVD was long thought of only as a passive, degenerative phenomenon (Rutkovskiy et al., 2017). However, as CAVD was studied more, there was a realization that it is in fact an active process involving changes in the cells located in the AV (Goldbarg et al., 2007; Pomerance, 1967). Disruption of the endothelial layer around the leaflet is believed to be a critical first step in the development of CAVD (Mohler, 2004). This allows immune cells, metalloproteinases, and possibly bacteria to enter the interior of the leaflet and induce changes (Rutkovskiy et al., 2017).

Metalloproteinases enter and slowly reorganize the valve's extracellular matrix causing thickening of the leaflets (sclerosis) (Rutkovskiy et al., 2017). Angiogenesis begins to occur, immune cells enter, and there is a build-up of cellular debris, lipids, and proteoglycans (Mohler, 2004; Chen & Simmons, 2011). Patients in this stage are usually asymptomatic (Rutkovskiy et al., 2017). This all leads to an inflammatory response that appears to be caused by both invading immune cells and local cells (Akat et al., 2009). Most AV calcification is thought to be a result of VIC differentiation into myofibroblasts (Rutkovskiy et al., 2017). This differentiation appears to be mediated by paracrine action from transforming growth factor β -1 (TGF β 1) (Xu et al., 2010). Contraction of the reorganized extracellular matrix by these newly differentiated

myofibroblasts leads to apoptosis of cell aggregates embedded in the matrix (Rutkovskiy et al., 2017). Sedimentation of calcium salts around apoptotic bodies, cleaved collagen type I chains, and cleaved elastin chains then occurs (Farzaneh-Far et al., 2001).

VICs can also differentiate into osteoblast-like cells. This differentiation pathway is largely promoted by Runt-related transcription factor 2 (Runx2) and bone morphogenetic proteins (BMPs) (Rutkovskiy et al., 2017). Once VICs are differentiated into this state, they begin secreting proteins such as osteopontin, osteocalcin, and alkaline phosphatase which are all expressed in high levels in bone tissue (Rutkovskiy et al., 2017). These osteoblast-like cells also begin organizing calcium crystals in the matrix into structures resembling lamellar bone (Rutkovskiy et al., 2017).

1.3 TGF β 1: Structure, Function, Signaling Pathway and Role in CAVD

TGF β 1 is a cytokine produced in both non-cardiac and cardiac tissue and is part of the TGF β superfamily which is collection of 33 genes that produce structurally related differentiation and growth proteins (Molin et al., 2003; Morikawa et al., 2016). The TGF β 1 ligand is a homodimeric signaling protein (Figure 1.5) (Hinck, 2012). TGF β 1, as well as its two sister isoforms, TGF β 2 and TGF β 3, are present only in vertebrates and have a bi-functional role in either inhibiting or activating cell proliferation in various tissues and organs, including the heart, during development and throughout life (Hinck, 2012; Morikawa et al., 2016). Additionally, TGF β 1-3 ligands are critical for wound healing and adaptive immune system regulation (O’Kane & Ferguson 1997; Letterio & Roberts, 1998). These three ligands are unique relative to other TGF β

superfamily ligands due to their ability to bind and signal via TGF β receptor type II (T β RII) (Akhurst, 2017).

The downstream results of TGF β 1-3 ligand binding are very contextual (Figure 1.6) (Akhurst, 2017; Liu et al., 2018). The pathway starts when one of the TGF β ligands binds to T β RII's extracellular domain (Shi & Massague, 2003). This leads to hetero-oligomerization of T β RII and TGF β receptor type I (T β RI), bringing about a conformational change to the newly formed receptor complex (Shi & Massague, 2003). Both T β RI and II are kinases that are a part of the tyrosine kinase-like family (Heldin & Moustakas, 2016). T β RII then phosphorylates and activates T β RI, which causes signal propagation either through the canonical Smad-dependent pathway and/or the Smad-independent pathways (Figure 1.6) (Derynck & Zhang, 2003). Interaction between TGF β and other signaling pathways involving growth factors and cross-talk between the Smad-independent and -dependent pathways leads to changes in Smad transcriptional output (Akhurst, 2017).

In the Smad-dependent pathway, it begins with T β RI becoming activated and phosphorylating Smad2/3 which recruits and binds Smad4 (Zhao & Chen, 2014). The Smad2/3-Smad4 complex then enters the nucleus where Smad3 and Smad4 bind to the Smad binding element on DNA and modulate production of transcription factors (Morikawa et al., 2013). Smad7 serves as an inhibitor of the Smad-dependent pathway (Zhao & Chen, 2014). There are a few different Smad-independent pathways. In these paths, activation of T β RI via T β RII binding to TGF β ligand results in activation of pathways such as phosphatidylinositol-3-kinase-AKT or mitogen-activated protein kinase pathway (ERK, p38) (Zhang, 2009).

As previously stated, there is cross talk between the Smad-dependent and – independent pathways. TGF β signaling is regulated by several mechanisms from the beginning, starting with transcription, until the end with release of the downstream products from the cell (Shi & Massague, 2003; Robertson & Rifkin, 2016). Ultimately, TGF β 1-3 ligand signaling results in expression of genes that are critical for process such as cell differentiation, cell matrix remodeling, apoptosis, and epithelial to mesenchymal transition (Gordon & Blobel, 2008; Morikawa et al., 2016).

TGF β 1 appears to play a role in the development and progression of CAVD. Tissue samples collected from both CAVD patients and non-CAVD patients were compared, and CAVD patients' tissue had greater levels of TGF β 1 (Jian et al., 2003). TGF β 1 levels were also higher in patients that were suffering from stenosis rather than the more serious sclerosis associated with greater calcification (Jian et al., 2003). Correlation does not mean causation though. The fact that TGF β 1 signaling plays a role in the remodeling of the cell matrix, cell differentiation, apoptosis, and transition of epithelial cells to mesenchymal cells, leads one to believe that it may be responsible for the changes that occur to VICs that promote the development CAVD. It is a prime candidate to study in hopes that non-invasive treatments for CAVD can be developed in the near future.

1.4 Specific Aims

The focus of this thesis is looking at the impact of sex hormones on the development of CAVD, and to research the potential of ethylenediaminetetraacetic acid (EDTA) as a non-invasive treatment for it.

Specific Aim 1: Understand the impact of sex hormones in the development of CAVD using TGF β 1 transgenic mice.

Specific Aim 2: Determine if targeted delivery of EDTA using nanoparticles can be utilized as a non-invasive treatment for CAVD.

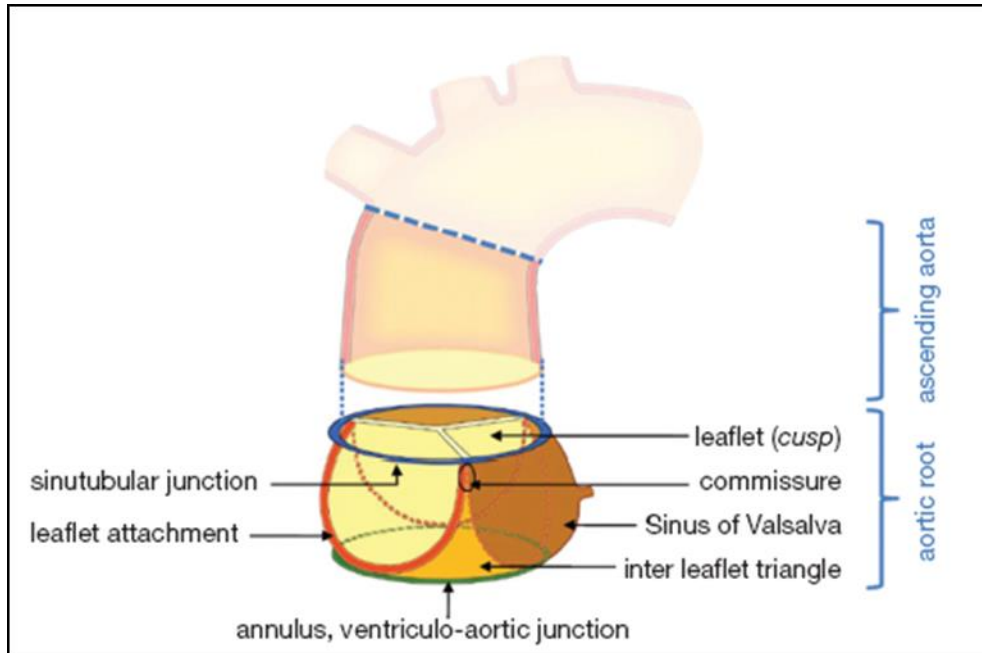


Figure 1.1 Anatomy of the Aorta. This figure depicts the structure of the AV. It exists from the output of the left ventricle until the sinutubular junction where it attaches to the ascending aorta. The AoR is composed of all the structure in the figure above, other than the ascending aorta. The AV specifically refers to the leaflets of the AoR. This image comes from Charitos & Sievers, 2013. Permission to use this image was granted by AME Publishing Company.

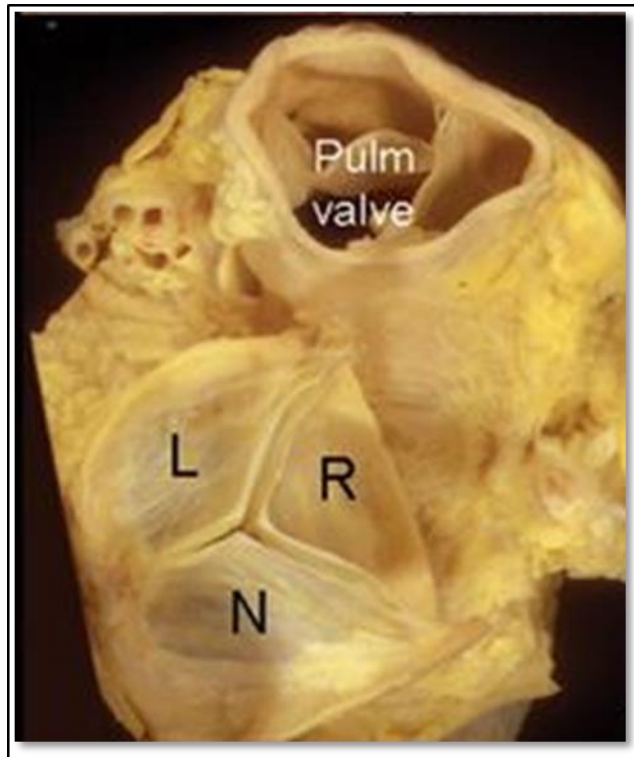


Figure 1.2 Diagram of Aortic Leaflets. This figure shows the left coronary leaflet (L), right coronary leaflet (R), and non-coronary leaflet (N) in relation to the Pulmonary (Pulm) trunk. This image was taken from Ho, 2009. Permission to use the image was granted by Oxford University Press.

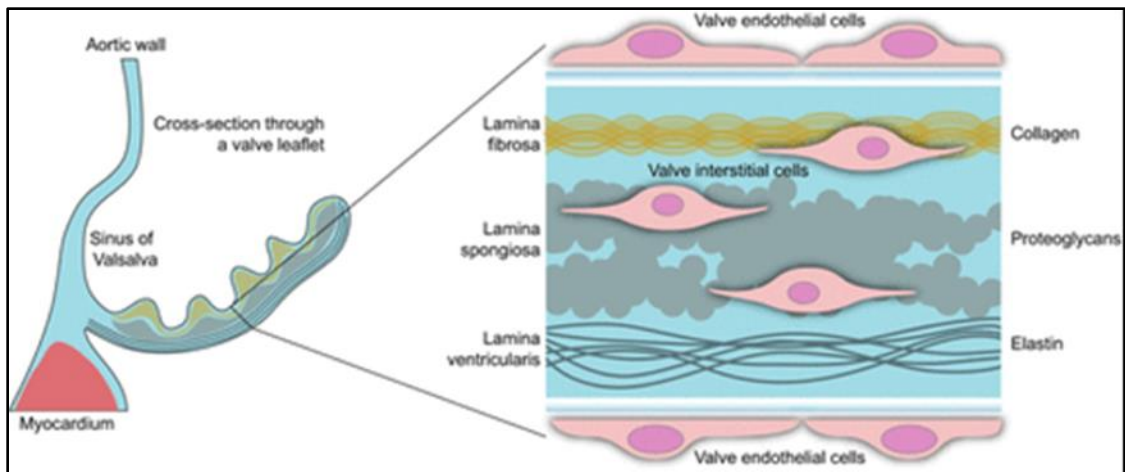


Figure 1.3 Cross Section of AV Leaflet. On the left, is an illustration of a cross section through the non-coronary AV. The image on the right shows the cellular composition of the AV leaflet.

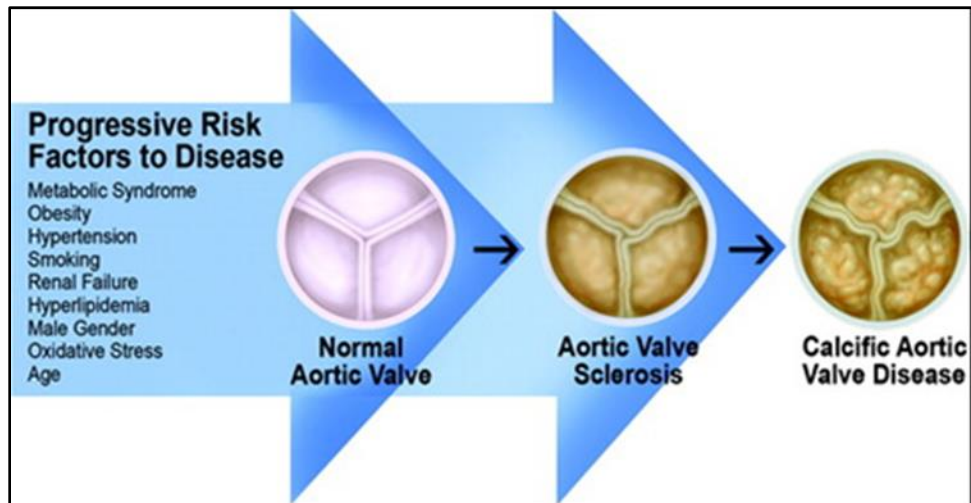


Figure 1.4 Progression of CAVD. This figure illustrates the progression of CAVD in the leaflets of the aorta from normal to completely calcified. Risk factors for the disease are list on the left side of the image. This figure was taken from Rajamannan et al., 2011. Permission to use this image was granted by Wolters Kluwer Health, Inc.

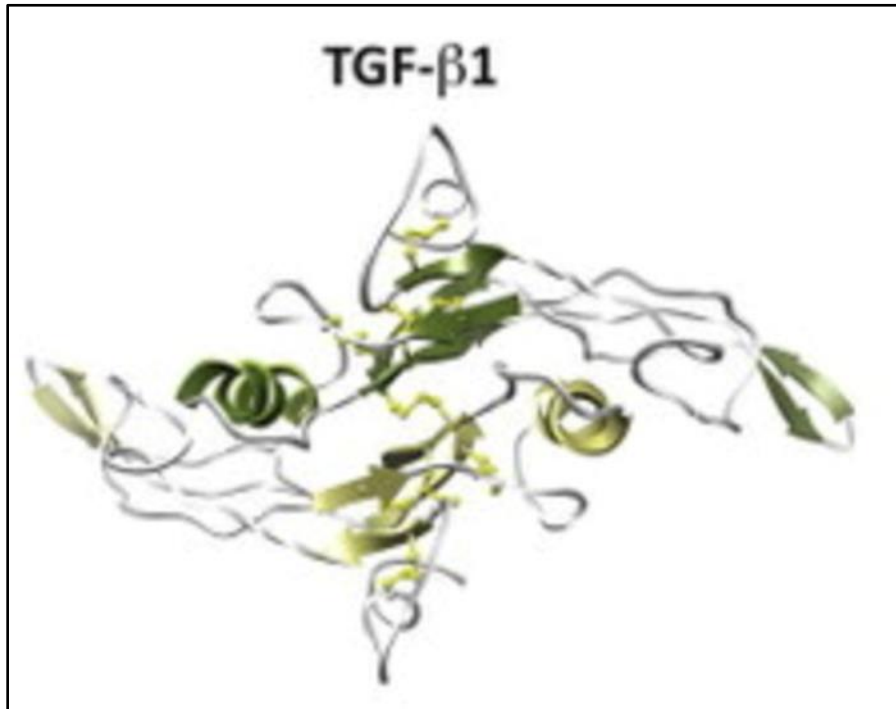


Figure 1.5 Structure of TGFβ1. This figure shows the homodimeric structure of the TGFβ1 protein. This image was taken from Hinck, 2012. Permission to use the image was granted by John Wiley and Sons.

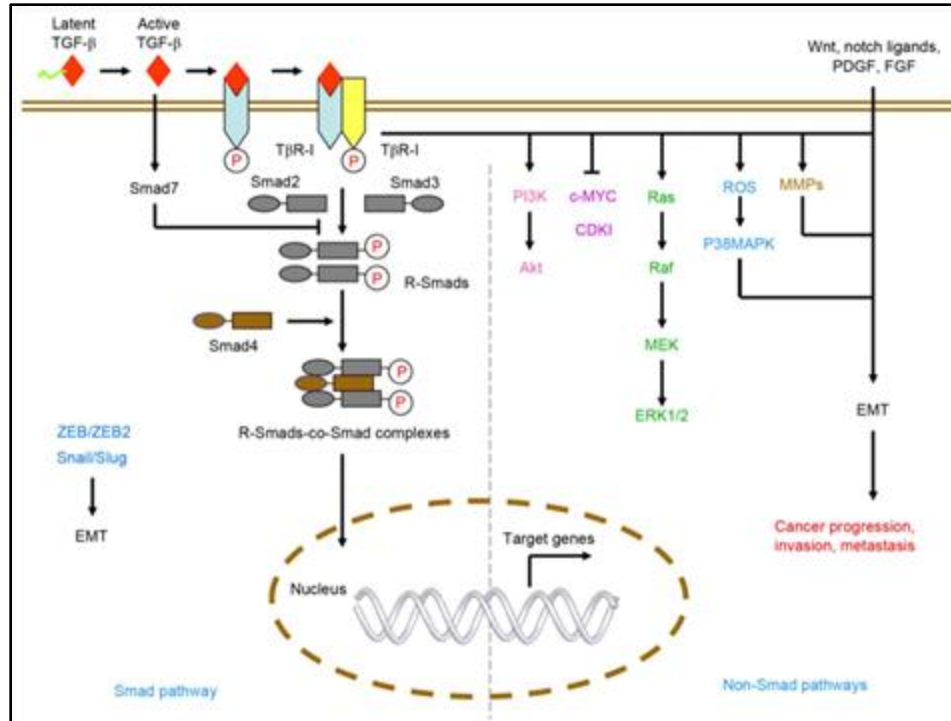


Figure 1.6 TGFβ Signaling Pathway. This figure illustrates a simple schematic of the TGFβ signaling pathway that results. It shows both the Smad-dependent and -independent pathways, as well as other growth factors modulating the activity of Smad transcriptional output in the non-Smad pathway. This image was taken from Liu et al., 2018. Permission to use the image was granted by Spandidos Publications.

CHAPTER 2

THE IMPACT OF SEX HORMONES IN CALCIFIC AORTIC VALVE DISEASE

Specific Aim 1: Understand the impact of sex hormones in the development of CAVD using TGF β 1 transgenic mice.

2.1 Introduction

A fairly novel area of study that could lead to greater understanding and possible treatment of CAVD lies in discovery of what causes male sex to be a risk factor for the disease. There are many cellular and molecular interactions that could explain why males are more prone to develop CAVD. One well established molecular aspect of CAVD, is that increased levels of the cytokine, TGF β 1, are present in the valve interstitial cells of calcified aortic valves (Jian et al., 2003). The exact molecular process to explain how TGF β 1 has this affect is unknown. It is also known that pre-menopausal women have a lower incidence of cardiovascular mortality than males, and that addition of exogenous estrogen can have anti-atherosclerotic effects (Ueda et al., 2019). This may mean that estrogen plays a protective role in cardiovascular diseases such as CAVD.

Additionally, testosterone may promote development of CAVD. However, the specific interactions between sex hormones and TGF β 1 signaling is a mystery.

Estrogen is a nonpolar steroid, so it can pass through the lipid bilayer and interact with receptors within the cell. Estrogen binds to estrogen receptors α and β (ER α and ER β) that are in the cytosol, and with estrogen binding proteins (EBPs) that are also

present in the cytosol (Kupier et al., 1997; Heldring et al., 2007). They also bind to membrane bound G-protein coupled estrogen receptors (Prossnitz et al., 2008). Through these interactions, estrogen has downstream effects that subdue molecular processes involved in calcification of cardiovascular tissue, such as suppression of p53 activity, decreasing NADPH oxidase activity, and dampening nuclear factor κ B (NF κ B) signaling (Zapata et al., 2005; Sahoo et al., 2015; Zhang et al., 2019). Estrogen also up-regulates processes that are protective against cardiovascular calcification such as increased expression of antioxidant enzymes and nitric oxide synthase (Figure 2.1) (Richards et al., 2013; Miller et al., 2008; Zhang et al., 2019). Testosterone is also a nonpolar steroid that directly enters the cell. Testosterone either directly binds to its intracellular receptor, androgen receptor (AR), or is converted to dihydrotestosterone (DHT) and then binds to AR (Davison & Bell, 2006). In terms of its impact in the development of CAVD, there have been numerous studies that implicate the downstream effects of AR activation in the promotion of calcification. Notably, these downstream effects include increased osteogenic signaling and increased levels of reactive oxygen species (Tuck & Francis, 2009; Chignalia et al., 2015).

Estrogen's interactions with TGF β 1 in the context of CAVD are not well understood. To make things more complicated, one must also account for BMP signaling which is tightly intertwined with TGF β signaling (Zhang et al., 2019). This further complicates the impact that estrogen may have in the development of CAVD, and research on the matter has only confirmed the complexity of these interactions. One study showed that estrogen decreased TGF β -dependent extracellular accumulation and non-

collagenous protein downregulation, both of which contribute to development of calcification (Donley & Fitzpatrick, 1998). Another study showed that estrogen can directly inhibit TGF β signaling by promoting degradation of Smad2/3 (Ito et al., 2010). However, other research revealed that estrogen promotes transcription of BMP2 (Zhou et al., 2003). BMP2 and its downstream effectors are pro-osteogenic and are strongly tied to induction of calcification in the aortic valve (Seya et al., 2011; Kaden et al., 2004). There is also evidence that Smad4, a signal transducer in the TGF β /BMP signaling pathway, can bind to ER α and inhibit estrogen signaling (Wu et al., 2003). Our understanding of how estrogen signaling is interwoven with TGF β /BMP signaling is limited and requires additional research.

The same can be said with testosterone signaling. There is some prior research in this area, but the results are limited and contradictory. As previously mentioned, some studies have shown AR activation, which can be induced by testosterone or DHT, can lead to promotion of calcification in cardiac tissue by increasing levels of reactive oxygen species and increasing osteogenic signaling. In Dr. Mohamad Azhar's lab, work with transgenic mice that have elevated levels TGF β 1 showed that CAVD developed in both sexes, but that the progression to aortic stenosis was more common in males. On the other hand, there is research that shows that testosterone and DHT can decrease calcification by inhibiting TGF β 1 signaling (Chung et al., 2014). Additionally, some research has shown that TGF β 1 induces activity of anti-osteogenic transcription factor, Sox9, and inhibits calcific nodule formation (Huk et al., 2016).

The goal of this study is to attempt to elucidate the effects of estrogen and testosterone to see what effect these interactions may have in the development and

progression of CAVD. There is limited work in this area and the results so far have been contradictory. The hope is that our work utilizing cell cultures and gonadectomies of mice will help add some insight into the effect of these steroid hormones have on the development and progression of CAVD. We will use TGF β 1/PeriostmCre transgenic (Figure 2.2) mice as an *in vivo* model. These mice produce greater amounts of TGF β 1 specifically in their VICs. It is well established that this mouse model develops CAVD based on years of work in Dr. Mohamad Azhar's lab. Female mice will undergo either ovariectomy (OVX) or sham OVX, and male mice will undergo either castration (CAST) or sham CAST. Work on this topic will also be studied *in vitro*. Cell cultures will use murine VICs that Dr. Mrinmay Chakrabarti isolated. It should be noted that these cells are not TGF β 1 transgenic cells.

2.2 Materials and Methods

2.2.1 Mice

All animal work was performed in accordance to protocol approved by the Institutional Animal Care and Use Committee (IACUC) at University of South Carolina. All mice were available in the Azhar laboratory. The mice used in this study were TGF β 1 transgenic (Tg), Postn-Cre Tg, or Postn-Cre non-transgenic (nTg). Additionally, some mice were membrane-targeted tandem dimer Tomato/membrane-targeted green fluorescent protein (mT/mG) transgenic. Mice in the preliminary study received a special chow that was high in fat. The nutritional composition of calories from this chow was 60% fat, 20% protein, and 20% carbohydrates. Mice in the OVX and CAST study were on normal chow.

2.2.2 OVX/Sham Surgeries

All animal work was performed in accordance to protocol approved by the Institutional Animal Care and Use Committee (IACUC) at University of South Carolina. Dr. Reilly Enos performed all ovariectomy, castration, and sham surgeries. To perform OVX surgery, the mice were anesthetized using isoflurane. 4% isoflurane was used for induction and 2% isoflurane and oxygen was used for maintenance of anesthesia. An incision was made first in the skin and then the muscle layers. Both uterine horns were tied with a 5-0 non-absorbable suture (category # S-G518R13). Then the ovaries were removed. For sham OVX surgeries, the ovaries were moved outside of the mouse's interior, but not removed. They were placed, intact, back into the abdominal cavity. For both sham and OVX, the muscle incision was sutured shut with 5-0 absorbable suture (category # S-G518R13-U) and the skin incision was closed using wound clips. A subcutaneous dose of Buprenorphine (0.43 mg/kg of bodyweight) was given as a pain reliever. One week after surgery, wound clips were removed (Bader et al., 2020). The procedure was similar for castration. In castration operations, the testes were removed via a midline excision and the ductus deferens were cauterized. The wounds were sutured in the same fashion as OVX surgeries and wound clips were also removed a week later.

Mice in the Preliminary OVX study underwent surgery at 7 months of age, while mice in the OVX & CAST study received surgery at 3-4 months of age.

2.2.3 microCT Imaging

microCT (mCT) scans were done on mice in this project to image and track the level of calcification in and around the aortic valve. First, the Perkin Elmer Quantum GX machine was turned on and allowed to warm up for 15 minutes. Once this was done, 1.5-

2% isoflurane was added to its appropriate containment and regulatory chamber, the oxygen supply was turned on, the vacuum pump system initiated, and the anesthesia muzzle was properly placed on the apparatus that holds the mice during the scan.

The mice were anesthetized in a box that circulated a mixture of oxygen and isoflurane. Once the mouse was anesthetized, it was quickly moved from this box into the Quantum GX. The mouse was then placed in a supine position, with its snout inserted carefully into the anesthesia muzzle. The Quantum GX door was then closed and the scan was started. All scans were done with the following settings: field of view (FOV) set to FOV45, High Resolution, 4 minute scan, X-ray filter of Cu 0.06+ Al 0.5. Once the scan was finished, anesthesia was stopped and the mouse was moved to a recovery cage. The images were saved and collected.

2.2.4 Echocardiography

Heart and valve function of the mice was tracked using echocardiography. A Vevo3100 with an MX400 transducer was the instrument used to achieve this. The transducer was positioned to achieve three primary views of the heart: Aortic Arch View (AAV), Parasternal Long Axis (PLAX) View, and Parasternal Short Axis (PSAX) View. To get the desired views of the heart, the MKT02620 Imaging Guides: Small Animal Echocardiography using the Vevo Imaging System Rev 1.0 was followed.

Before imaging of the heart, the mice were anesthetized in a box that circulated a mixture of oxygen and isoflurane. Once the mouse was anesthetized, protective lubricant was placed over its eyes, and then the mouse was laid on the imaging platform and had its snout placed into the anesthetizing tube. Once there, its hands and feet were placed onto the sensors that tracked heart and breathing rate and fastened down with tape. Heart rate

was maintained at a rate greater than 400 beats per minute. The mouse's hair was removed from its chest and upper abdomen using Nair. Once the hair and Nair were appropriately washed away, gel was placed onto the transducer and imaging could begin.

To acquire the PLAX and PSAX View, the imaging platform the mouse was on was tilted down slightly. The transducer was placed such that the notch on the transducer was pointing towards the mouse's head and the rotated approximately 35° counter clockwise. From this view data could be collected for PLAX. To transition from collecting data in the PLAX view to the PSAX view, the transducer was rotated 90° clockwise from the PLAX View. In these two views, M-Mode data was collected.

To acquire data relating to the aortic valve function, the right side of the imaging stage was titled down, and the transducer was placed on the left side of the mouse such that the notch was pointing towards the mouse's head and was parallel with the chest to achieve AAV. The transducer was moved and angled until a good view of the aortic arch was achieved. The innominate, subclavian, and left common carotid arteries served as landmarks to help achieve this view. In this view data relating to blood flow was collected using Color Doppler and PW Doppler.

To measure and quantify AV function, data was collected using Doppler imaging and collection of data on peak pressure (mmHg) and peak velocity (mm/s) of the AV. The normal flow of blood across the AV in mice at peak systolic velocity is <10 mmHg and normal peak aortic velocity (mm/s) is 900-1500 mm/s (Miller, et al., 2011; Casclang-Verzosa et al., 2017). Peak aortic velocity great than 5000 mm/s has been associated with severe aortic stenosis (Casclang-Verzosa et al., 2017).

2.2.5 Tissue Collection and Processing

At the end of the studies, mice were sacrificed by being placed in a chamber containing isoflurane. Once deceased, its heart was retrieved from the body and placed in a vial containing 4% paraformaldehyde for 24-48 hours. The heart was then held in 70%, 95%, and 100% ethanol for 24 hours each. After this, the vial containing the heart was filled with xylene and placed in a vacuum oven at 60 °C for three hours. This was done twice with a change into new xylene for the second three hour period. After that, the heart was left overnight in a 50% xylene, 50% paraffin mixture. The next day, the xylene-paraffin mixture was melted, removed, and replaced with 100% paraffin in the vial. The vial was then be placed in the vacuum oven at 60 °C for 4 hours. After 4 hours, the vial was removed from the oven and the heart was held overnight in this paraffin. The next day, the vial was placed into the vacuum oven at 60 °C for two 4 hour periods, with a change of paraffin before the second period. Once this was done, the heart was placed into a mold and was ready to be sectioned, placed on microscope slides, and exposed to various histological staining. Alternatively, some hearts underwent processing for cryostat sectioning. In this case, the hearts were placed in a vial containing paraformaldehyde for 24 hours. The next day, they were washed three times with 1X phosphate buffered saline (PBS), and then, placed in sucrose for 24 hours. Once sucrose saturation was complete, the hearts were again washed three times with PBS. After the PBS wash, the hearts were placed in Optimal cutting temperature (OTC) compound and stored in a -40°C refrigerator for at least 24 hours.

2.2.6 Alizarin Red Staining of Tissue Samples

Before any of the microscope slides with tissue sections could be stained, they first had to be deparaffinized in three washes of xylene for 3 minutes each. The tissue was then hydrated. To achieve this, slides were placed in two washes of 100% ethanol for 2 minutes each, then in 95% ethanol for a minute, 70% ethanol for a minute, and then were gently washed in deionized water for approximately a minute.

Next, for Alizarin Red Staining, Alizarin Red solution was placed directly onto the tissue sections using a pipette to carefully add drops of the staining solution until it covered the section. The staining solution stayed on the section for 5 minutes. After 5 minutes, the Alizarin Red solution was completely removed from the tissue section. The slide was then placed in acetone for 1 minute, and then a 50/50 mixture of acetone and xylene for 15 seconds. The slide was then cleared in three changes of xylene for three minutes in each change. Finally, the slide was air dried and a coverslip with permanent mounting media was placed over the tissue section.

2.2.7 Cell Culture and Alizarin Red Staining and Quantification of Cell Cultures

VICs were grown at 33°C in Dulbecco's Modified Eagle Medium (DMEM) media containing 10% Fetal Bovine Serum (FBS), 1% penicillin-streptomycin, Glutamine (1 mM) and γ -interferon (10 units/ml; Peprotech INC.; catalog: 315-05). Once cells are ~80-90% confluent, they were seeded in six well plates (2×10^5 cells/well) in quadruplicate for each treatment at 37°C without γ -interferon. Cells are grown either in DMEM media or osteogenic (OST) media. OST media is composed of Hi glucose DMEM, 10% FBS, 1% P/S, 10 nM L-beta-glycerolphosphate, and 50 μ M ascorbic acid. provided by CBA Cell Culture Lab for 14, 21, or 28 days in presence or absence of 1 μ L

of either 100 nM Estradiol (E) or 100 nM Di-hydro Testosterone (DHT) dissolved in Dimethyl sulfoxide (DMSO). We changed the media/drugs every 5 days during course of the experiments. At the end of the treatments, cells were washed thrice in Phosphate Buffer Saline (PBS) and Alizarin red staining was performed to determine calcification in the cultured cells as follows.

The cells were fixed using 4% paraformaldehyde for 15 min at room temperature. Before staining, fixed cells were washed thrice with deionized water. Then 500 μ l of Alizarin red solution (American Mastertech Scientific Inc. Cat # STARE100) was added to each well of the six well plate and incubated 30 min with gentle shaking. At the end of the incubation, VICs were washed with deionized water six times, air dried and photographed using a Carl Zeiss camera at either 4X or 10X magnification of each well, making sure that we randomly chose 5 fields from each well. ImageJ software was used to quantitate each image after setting up the scale, RGB stack, and threshold values. We always use the same threshold for all the images in the experiment. Then Alizarin red stained areas were measured for each images keeping similar setting for the software. We measured the percentage of stained area as our record, then calculated relative changes in staining area following different media/drugs and presented graphically.

These cell cultures were only done once. There were no duplicate or triplicate studies.

2.2.8 Quantification and Statistical Analysis of Data Collected

Color thresholding in the NIH software, ImageJ, allows one to quantify calcification captured within a live mouse during mCT scans. This is achieved when pixels of an individual image within a stack of hundreds of images (collected during a

scan) are counted using an interactive image-altering technique called, Color Threshold. The calcified nodule will appear white, similar to bone, in a normal mCT image. To quantify the presence of calcification, one must change the color threshold settings until bone-like material, but not tissue, appear red. This indicates that pixels are being tagged onto bone-like material. Those pixels can then be counted. Once the nodule is located, one can set parameters to measure specifically in the area around the nodule and begin quantifying the level of calcification. Measurements are taken for as much of the calcified area as possible where pixels are being tagged to the calcification.

Quantification of ECHO data was done using FujiFilms VEVO Analysis software provided by the Instrument Resource Facility at U of SC School of Medicine-Columbia. Statistical analysis was conducted in GraphPad Prism 9. All Statistical Analysis was done using GraphPad Prism 9. Two-way ANOVA with multiple comparisons and a Tukey test were done to determine statistical significance between treatment groups in the OVX and CAST study.

2.3 Results

2.3.1 Preliminary Research Indicates Development of Calcification at a Greater Rate after Ovariectomy

In the preliminary study there were 4 female mice: 2 received sham surgeries and 2 underwent ovariectomies (OVX). The 2 OVX mice were TGF β 1 double transgenic (dTg) and had elevated levels of TGF β 1 in their aortic valves (AVs). One of the mice that received a sham surgery was dTg while the other was non-transgenic (nTg). The nTg mouse was not overproducing TGF β 1 in its AV (Figure 2.3).

The development of calcification was tracked in these mice using microCT (mCT) imaging. The mice were given one month to heal from surgery and consume a high fat diet (HFD). The purpose of using the HFD was to expedite the development of calcific aortic valve disease (CAVD) as obesity is a major risk factor for the disease. After the one month, the mice were scanned once every two weeks (except for a period of four weeks where the mCT machine was undergoing repairs).

The scans (Figure 2.5) were collected, and calcification of the AV was quantified in ImageJ. The first mCT scan revealed that one of the OVX mice had calcification and the TGF β 1 dTg mouse that received a sham surgery had calcification. This trend remained until the final scan which revealed that the other OVX mice had developed CAVD (Figure 2.4). The TGF β 1 nTg mouse did not calcify throughout the course of the experiment. It did gain the most weight though (Figure A. 1).

Alizarin Red staining was done on tissue sections collected from each mouse to confirm that there was calcification (Figure 2.5). The Alizarin Red staining was consistent with the information collected from the mCT imaging.

2.3.2 Echocardiography Indicates That Calcification Has Negative Effects on Blood Flow through the AV

Echocardiography imaging and data further confirmed the development of CAVD in the dTg mice that had calcification in the AV. To determine AV function, data was collected using Doppler imaging and collection of data on peak pressure of the AV (mmHg). Irregular blood flow was seen in all dTg mice AV, regardless of the type of surgery (Figure 2.6). The blood flow through the AV of the non-calcified mouse was normal (Figure 2.6). This was confirmed quantitatively (Figure 2.7). The normal flow of

blood across the AV in mice at peak systolic velocity is <10 mmHg. 1.5 months after surgery, the nTg Sham OVX mouse had a peak AV pressure of 2.291 mmHg, the dTg Sham OVX mouse had a peak AV pressure of 2.690 mmHg, and the average peak AV pressure of the 2 OVX mice was 5.323 mmHg (Figure 2.7). 3 months after surgery, the peak AV pressure of the sham nTg OVX mouse was 2.323 mmHg, the dTg Sham OVX peak AV pressure increased from 2.690 mmHg to 15.303 mmHg, and the average peak AV pressure of the dTg OVX mice increased from 5.323 mmHg to 13.513 mmHg (Figure 2.7).

2.3.3 Estrogen is Temporally Protective against Calcification *in vitro* for Female VICs

Cell culture work was done using six 6 well plates. There were three sets of plates populated by male murine VICS (Figure 2.11) and three sets of plates with female murine VICs (Figure 2.9). One set of each of the male and female plates was followed for 14 days, another for 21 days, and a final set for 28 days. On each of these six plates, four wells were used: one well was covered DMEM, one OST, one OST+E, and one OST+DHT.

Data collected from the 14 and 21 day cell culture experiments of female VICs was nearly identical (Figure 2.8). In both cell cultures, calcification (measured by the % of area calcified relative to not calcified) was detected in the wells with OST, OST+E, and OST+DHT media, but none was present in the well containing DMEM media (Figure 2.8). The % of area calcified in the well with OST media for the 14 day culture was 14.03% (Figure 2.8). This was greater than both DMEM and OST+E (Figure 2.8). The average % of area calcified in OST+E media for 14 days was 0.48% (Figure 2.8).

However, the % of calcified area in the OST media was less than that of the OST+DHT media, which had an average value of 24.93% calcified area (Figure 2.8). The data collected in the 21 day media was practically identical. The OST media showed a greater % of area calcified relative to both the DMEM and OST+E wells, while the OST+DHT well calcified (24.59%) more than the OST media (Figure 2.8). There was no difference between the DMEM and OST+E media at either 14 days or 21 days (Figure 2.8). The mean values were within the same standard deviation.

The results seen in the previous two cell cultures were not seen in the 28 day cultures. In this portion of the study, the OST and OST+DHT wells were not different in terms of the % of calcified area (Figure 2.8). They were within each other's standard deviation. Additionally, while both OST and OST+DHT were more calcified than the OST+E well, the amount of calcification present in the OST+E well had increased relative to the 14 day and 21 day wells with E (Figure 2.8). The 28 day well with OST+E had an average % of calcified area of 16.48% (Figure 2.8). That is a little over a 5000% increase from the 21 day OST+E well which had an average % of calcified area of 0.32% (Figure 2.8).

2.3.4 Male VICs Calcify *in vitro* Regardless of Hormone Treatment

The results seen in the male VIC cultures (Figure 2.11) were quite different compared to their female counterparts. Calcification was pervasive throughout the OST media, regardless of treatment or exposure to DHT or E. There was no difference in the mean values of the % of calcified area in OST, OST+E, and OST+DHT in the 14, 21, or 28 day cell cultures (Figure 2.10). All were within each other's standard deviation. The only difference of note was a temporal difference between the average % of calcified area

of the OST well at 14 days and 28 days (Figure 2.10). The 14 day well had a mean value of 24.85% while the 28 day well's mean value was 41.98% (Figure 2.10). The rest of the temporal comparisons between wells and treatment were not different as they all were within each other's standard deviation.

2.3.5 Development of CAVD in Mice Regardless of Surgery in OVX & CAST Study

A follow-up *in vivo* mouse study was conducted to further explore the impact of sex hormones on the development of CAVD. This project would include both female mice (n=7) and male mice (n=4). The surgery types remained the same for females. They either received OVX (n=5) operations or sham OVX (n=2) operations. Males received either CAST (n=3) or sham CAST (n=1).

Data from mCT scans done before the operation and three months after the operations. To compare the data and determine significance, a 2-way ANOVA multiple comparisons with Tukey test was conducted. This test revealed that there was no significant difference in average mean calcification (AU) data collected pre-operation when comparing one of the four groups to the other (Figure 2.13). The same results were found for the average mean calcification of the four groups at the end (Figure 2.13). The only statistically significant phenomenon observed according to this test was when average mean calcification of the OVX group was compared pre-operation vs three months after operation ($p=0.037$) (Figure 2.17). While the sample size of the sham CAST group is n=1, it should be noted that mean calcification of this group increased from 31.60 AU to 130.7 AU which was very similar to the increase seen in the OVX group (43.88 AU to 136.03 AU) that was deemed statistically significant (Figure 2.13).

These non-significant results were further confirmed by mCT scans of just the heart tissue that was collected after the mice were sacrificed. With less tissue and bone in the way of the scan, it was an opportune time to specifically focus on calcific nodule located in the AV. The volume of the nodule was measured utilizing the orthogonal view of the heart. Similar to the results seen in mean calcification three months after operation, there was no significant difference between the four groups in terms of the average volume (mm³) of the nodule (Figure 2.13).

2.3.6 Echocardiography Indicates That Calcification Has No Significant Effects on Blood Flow through the AV

As in the preliminary OVX study, echocardiography imaging and data was collected. However, in this study, according to two-way ANOVA multiple comparisons with Tukey tests, there was no significant change in the average peak AV pressure (mmHg) or peak AV velocity (mm/s) before or after surgery (Figure 2.15). None of the average nor individual values of any of the four groups or individual mouse within those groups exceeded the normal peak AV pressure of 10 mmHg or normal peak AV velocity of <1500 mm/s (Figure 2.15). However, Doppler imaging showed turbulent blood flow in the AV of most of the mice before surgery, and in all of the mice after surgery regardless of which surgery they underwent (Figure 2.14).

2.4 Discussion

Based on the results of these three studies, it appears that estrogen may play a protective role in preventing development of CAVD in female VICs, but this is only true when TGFβ1 is not overexpressed. In the preliminary OVX study, both mice that were dTg and OVX developed CAVD, the dTg sham OVX mouse developed CAVD, but the

nTg sham OVX mouse did not. The sham OVX mouse that did develop CAVD had upregulated levels of TGF β 1, just like the OVX mice. Estradiol (E) alone was not enough to prevent CAVD. This seems to indicate that any possible protective effects of estrogen are lost when there is an excessive amount of TGF β 1. This theory seemed to be confirmed by the OVX & CAST study. All mice in this study were dTg. The females were all dTg and developed CAVD after both sham and OVX surgeries, which is what was observed in the preliminary study.

This conclusion is consistent with observations from in vitro experiments. In cell culture experiments, significant calcification developed in female VICs when they were in OST and OST+DHT wells in 14, 21, and 28-day cultures. However, in all three of the OST+E wells calcification was significantly suppressed relative to their OST and OST+DHT of the same time. The OST+E wells were not different than the DMEM media in the 14 and 21-day cultures. Even in the 28-day cell culture wells, while the OST+E well calcification levels were higher than the DMEM well, the OST+E well remained less calcified compared to the OST and OST+DHT wells. These VICs are not dTg, so they do not have elevated levels of TGF β 1 to outweigh the protective effects of E.

This seems consistent with some previous research. Donley & Fitzpatrick (1998) showed that estrogen prevents CAVD-inducing processes such as accumulation of TGF β -dependent extracellular materials and non-collagenous protein downregulation. Later research showed that estrogen can promote degradation of Smad2/3 which is a critical part of TGF β signaling (Ito et al., 2010). One of these pathways may explain what was seen in the nTg mouse that underwent sham surgery. Her resistance to CAVD may have

been two-fold: she had sufficient levels of estrogen and normal levels of TGF β 1. It is even possible that her estrogen levels were higher considering she weighed more (Figure A. 1) and was on a high fat diet. It is well known that fat cells produce estrogen. However, the *in vivo* hormone concentrations were not measured in any of the mice so this is conjecture. Hormone concentrations of mice need to be monitored in later research.

All dTg female mice developed CAVD regardless of whether they underwent sham or OVX surgery. The molecular equilibrium appears to have been pushed in favor of TGF β /BMP signaling pathway over the estrogen pathway as all three had calcific nodules. A previous study showed that a signal transducer in the TGF β /BMP signaling pathway, Smad4, can bind to estrogen receptor- α (ER α) and inhibit estrogen signaling (Wu et al., 2003). There may be competitive inhibition occurring where increased TGF β /BMP signaling leads to greater quantities of Smad4 which is then able to outcompete estrogen for ER α , thus preventing any protective effects in sham OVX females. The fact that the sham dTg mice developed CAVD and that nTg VICs in cell culture did not calcify in the presence of E gives credence to this idea of competitive inhibition of ER α leading to calcification. More detailed research needs to be done at the molecular level utilizing techniques such as western blot and qPCR.

The potential for protective effects of estrogen in males does not appear to be as optimistic. Decreasing testosterone does not appear to prevent CAVD either. All the dTg male mice calcified, regardless of whether they underwent CAST or sham CAST surgery. It must be noted that conclusions *in vivo* should be taken skeptically, as the sample size for the CAST (n=3) and sham CAST (n=1) were small. Additionally, *in vitro*, there were

no significant differences between 14, 21, or 28-day wells in any version of the OST wells. Every OST, OST+DHT, and OST+E well calcified at all three time intervals. E does not appear to have protective effects when it comes to preventing calcification of male VICs.

The development of pervasive calcification in OST wells of male VICs is not surprising as it was a positive control for calcification development (the same is true for female VICs). Males are at a much higher risk of developing CAVD (O'Brien, 2007; Yutzey et al., 2014). Decades of work done by Dr. Azhar has shown that male mice are at the same risk as humans for CAVD development. Testosterone seems to be the obvious explanation for this risk, but the data from these studies brings that into doubt. qPCR analysis done by Dr. Reilly Enos' lab (Figure A. 3) showed that there are no statistically significant differences in ER α expression between male and female control and TGF β 1 Tg mice. This paired with the results of this set of studies is interesting. These male and female mice and VICs are likely expressing the same amount of ER α , so it is unlikely that this receptor alone provides an explanation. Both male and female mice calcified heavily in the presence of DHT. DHT cannot be converted to estrogen by aromatase, so only AR activation can be considered here. It is possible that male VICs have lower expression of EBPs and/or GPERs relative to female VICs and that activation of one or both of these receptors is the key to E having protective effects.

In conclusion, the results of these studies indicate that E plays a protective role in preventing the VICs of females, whereas testosterone promotes calcification of female VICs. For male VICs, estrogen has no protective role against calcification and leads to the same amount of calcification as testosterone. In vivo, the protective role of estrogen

in female mice is outweighed by the pro-osteogenic effects of increased levels of TGF β 1 in the VICs of the AV. More research is needed as there is not much literature available on the interaction of sex hormones and TGF β 1 in the development of CAVD. Future research on the area should measure the blood concentration of hormones in female and male mice that undergo gonadectomies or sham procedures and data using techniques such as qPCR and western blot needs to be done to provide clarification on what may be occurring at the molecular level.

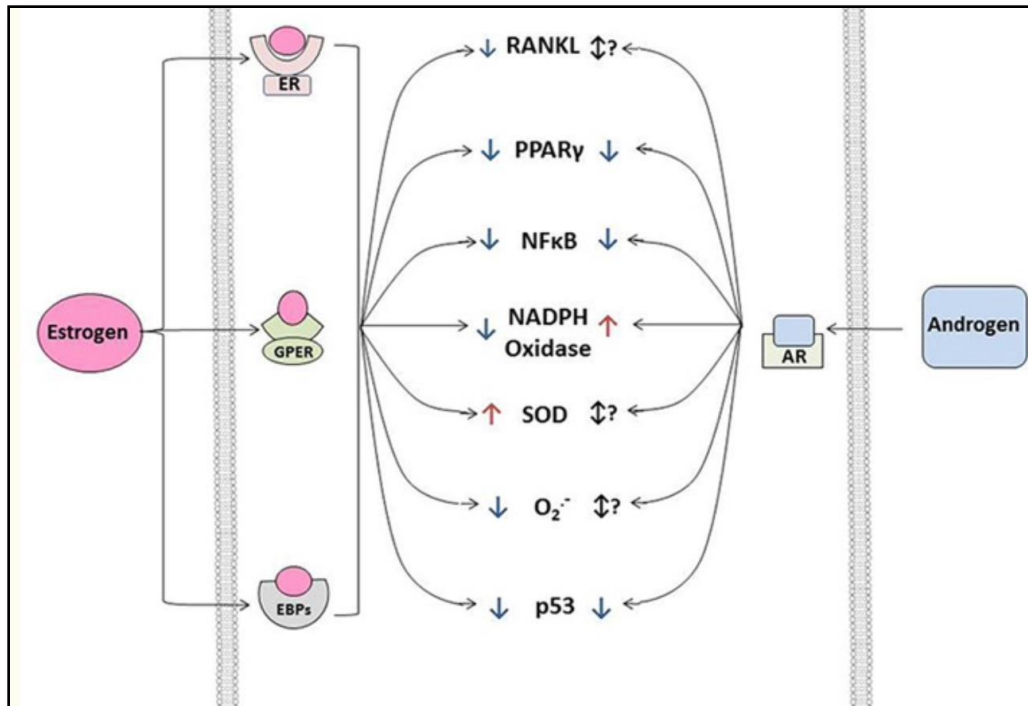


Figure 2.1 Estrogen and Androgen Signaling. This diagram illustrates the effects that estrogen and androgen signaling have in various cellular processes that are believed to be involved in the regulation of cardiovascular calcification. Estrogen is shown binding to an estrogen receptor (ER), a G-protein coupled estrogen receptor (GPER), and to estrogen binding proteins (EBPs), while androgen is shown binding to an androgen receptor (AR). These interactions have downstream effects within the cell. They are either positive (up arrow) and/or negative (down arrow) or the effect is unknown (up and down arrow with question mark). The molecules shown to be influenced by sex hormones are: RANKL, receptor activator of nuclear factor κ B ligand (promotes calcification); PPAR γ , peroxisome proliferator-activated receptor- γ (prevents calcification); NF κ B, nuclear factor κ B (promotes inflammation/calcification); NADPH oxidase, nicotinamide adenine dinucleotide phosphate oxidase (increases oxidative stress/calcification); SOD, superoxide dismutase (reduces oxidative stress/calcification); O₂^{•-}, superoxide anion (increases calcification); p53, tumor protein 53 (promotes inflammation/calcification). This figure was taken from Zhang et al., 2019 which is an open-access article.

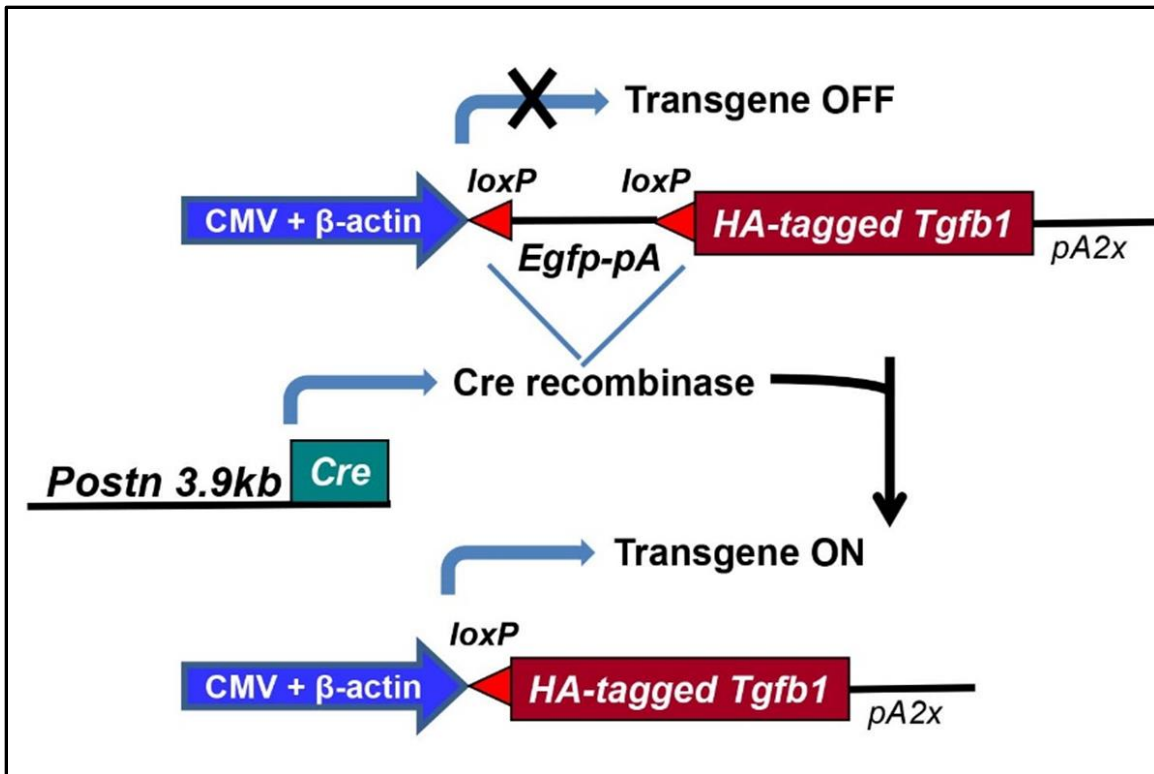


Figure 2.2 Diagram of TGFβ1 Transgenic Mice Genetic Model. This is a schematic explaining at a genetic level how the transgenes of TGFβ1/PeriostmCre double transgenic mice were designed and function. An Egfp-pA intervening sequence places the HA-tagged TGFβ1 cDNA away from the promoter which turns the TGFβ1 transgene (Tg) off. PostnCre Tg mice have a recombinase enzyme under control of the Postn3.9 Kb promoter expressed by VICs. LoxP sequences are recognized by Cre recombinase and delete the Egfp sequence which then activates the TGFβ1 gene. This image was produced by Dr. Azhar. Permission to use was granted.

Mouse	Genotype	Date of Birth	Type of Surgery
3864	TGFβ1 ⁺ ;PeriCre ⁻ (nTg)	10/23/20	Sham
3869	TGFβ1 ⁺ ;PeriCre ⁺ (dTg)	10/25/20	Sham
3870	TGFβ1 ⁺ ;PeriCre ⁺ (dTg)	10/25/20	OVX
3871	TGFβ1 ⁺ ;PeriCre ⁺ (dTg)	10/25/20	OVX

Table 2.1 Genetic Background of Mice. This table provides background information on the 4 mice in the preliminary OVX study. The first column provides the identification number of the mice. The second column gives the genetic background of the mice. Specifically, that all were positive (+) for the double transgenic (dTg) TGFβ1/PeriCre transgene, and one mouse (3864) was negative(-) for the PeriCre transgene (nTg). This means that the TGFβ1 transgene in this mouse was not activated. The third column provides their date of birth, and the fourth column indicates which type of surgery they underwent. Sham surgery did not result in the removal of the ovaries from the mice, whereas ovariectomy (OVX) surgery did.

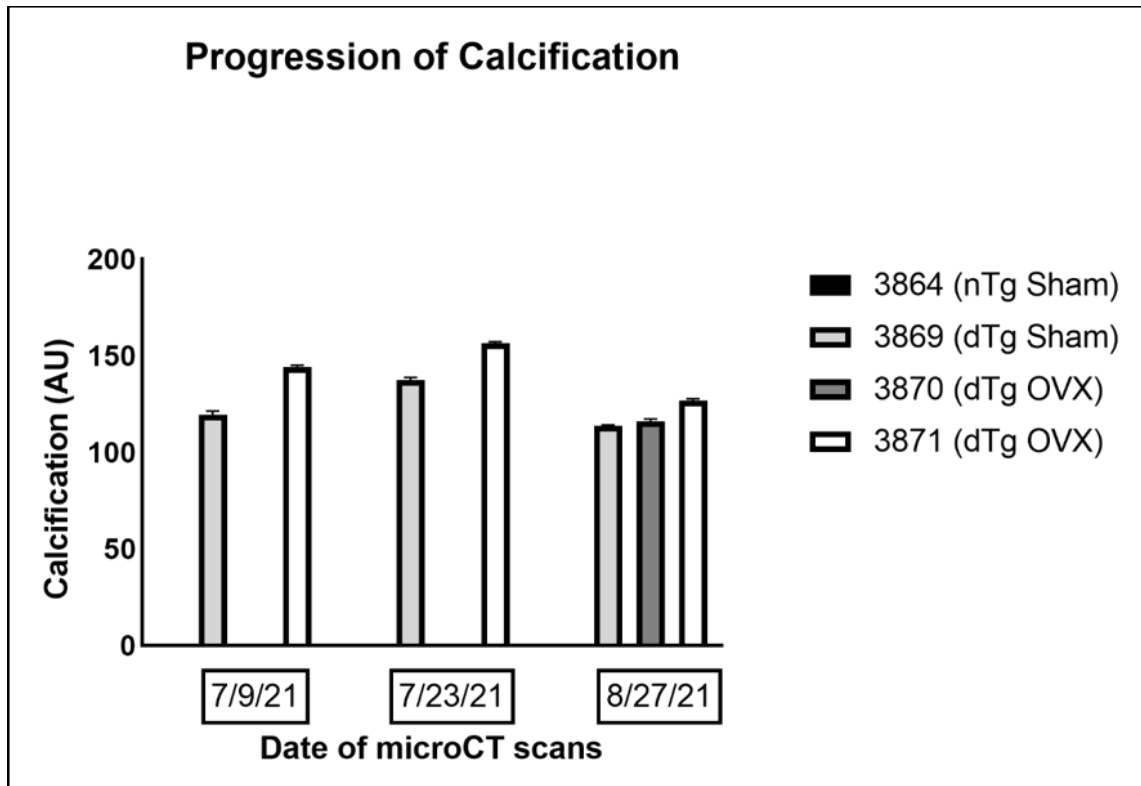


Figure 2.3 Quantification of Calcification via mCT Imaging of Preliminary OVX Study. This image shows the development of calcification over the course of the three month study for each individual mouse (n=4). The legend on the right side of the graph shows the identification number of mouse, as well as whether it was non-double transgenic (nTg), double transgenic (dTg), and if the mouse underwent sham or ovariectomy (OVX) surgery. The legend also shows the color associated with the tracking of each mouse's calcification over time. The date of the scan being quantified is shown on the x-axis, and the y-axis shows the average (n=5 for each bar) number of pixels detected (AU) and quantified in ImageJ using color thresholding technique.

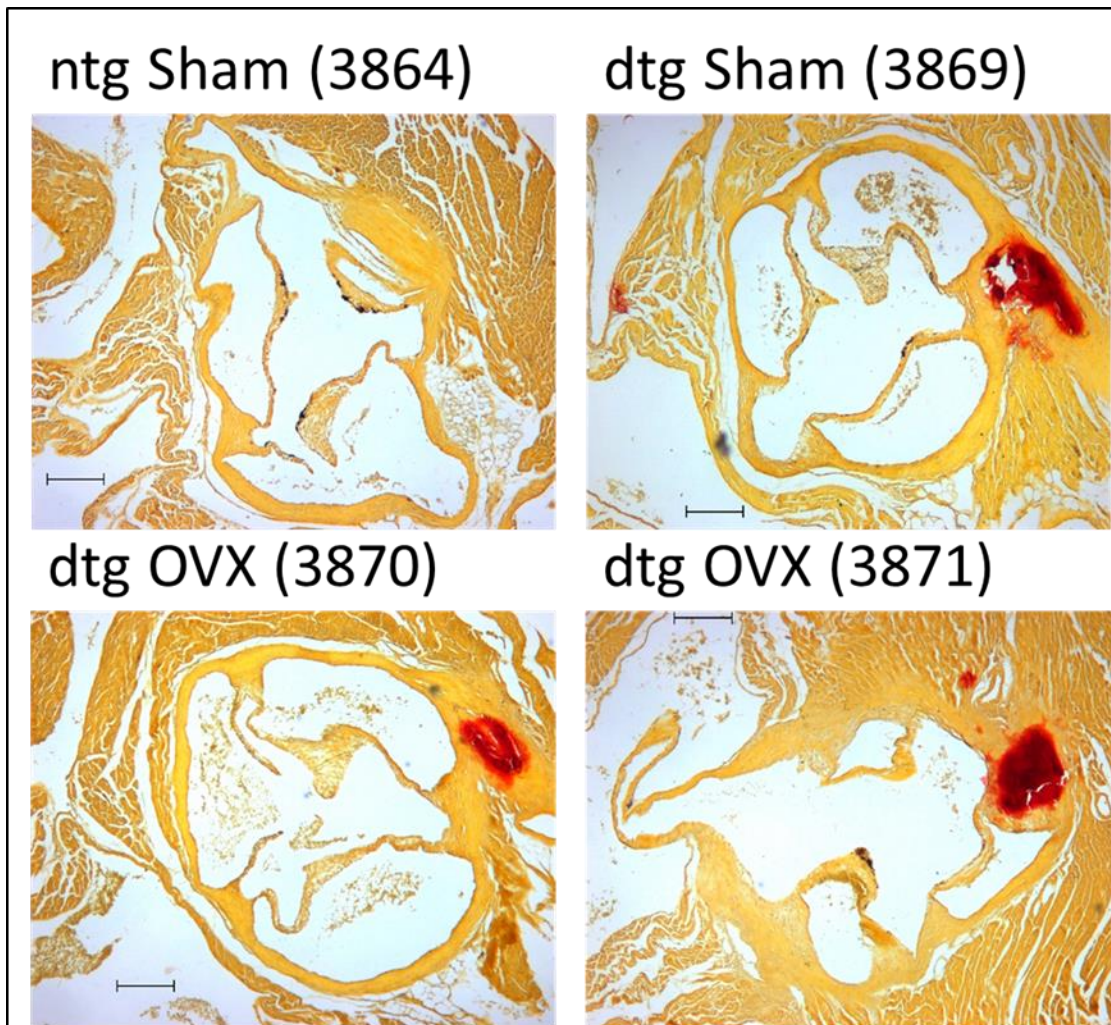


Figure 2.4 Alizarin Red Staining of the AVs of Preliminary OVX Study. Alizarin Red Staining confirms the presence of calcification in and/or around the AV of 3 of the 4 mice. Information above each image provides the identification number of mouse, as well as whether it was non-double transgenic (ntg), double transgenic (dtg), and if the mouse underwent sham or ovariectomy (OVX) surgery. Areas of calcification stain red when exposed to Alizarin Red staining. Each image was captured using a Carl Zeiss camera attached to a microscope in 4X magnification. Each image has a 200 μm scale bar.

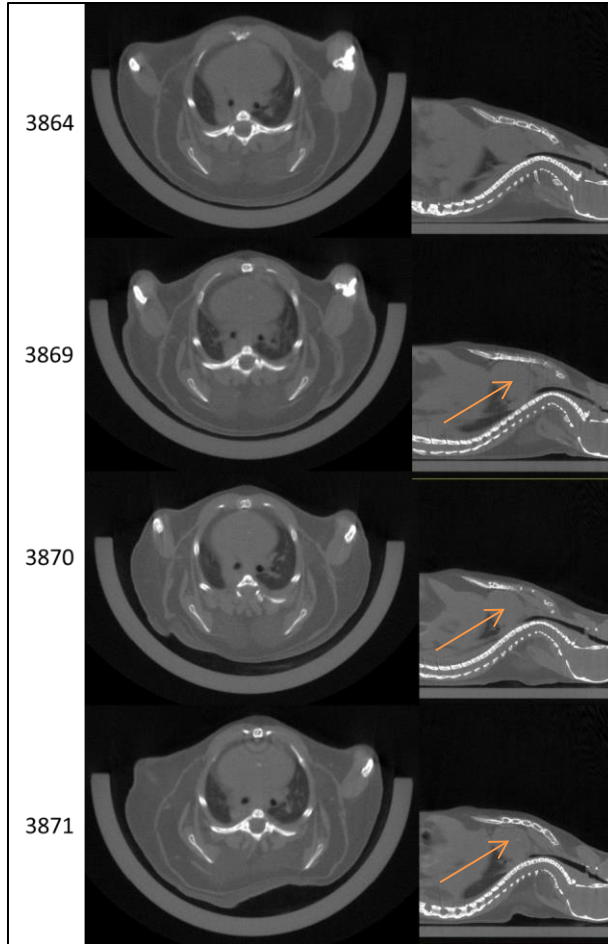


Figure 2.5 mCT Imaging of Each Mouse in Preliminary OVX Study. Left-to-right are images from approximately the same XZ-axis and YZ-axis location in the same mouse collected during 4-minute, FOV45 scans using a Perkin Elmer Quantum GX. These images were collected at the end of the three month experiment. There is an orange arrow pointing to the calcification located around the AV.

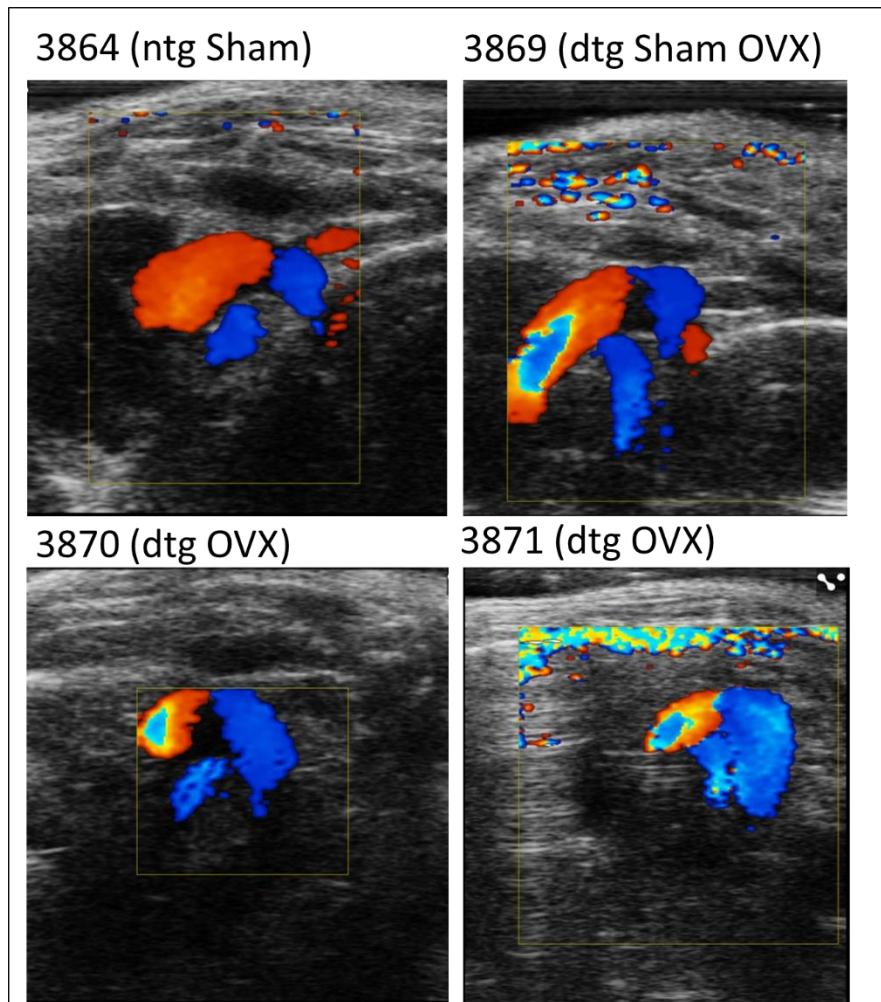


Figure 2.6 Doppler Imaging of AV from Preliminary OVX Study. These are representative images of the AV of mice (n=4) captured using a Vevo3100 with an MX transducer. The transducer was positioned in the Aortic Arch View (AAV) to achieve a view of the aortic valve. Doppler imaging is a colorful visual representation of direction of blood flow. Red indicates that blood is flowing towards the transducer, while blue indicates that it is flowing away from the transducer. The image in the top left shows proper blood flow. Blood is passing through the aortic valve (red) and then moving down the descending aorta (blue). The other three images show turbulence in movement of blood specifically at the AV. This indicates there is constriction of blood flow at the AV. This is a common indicator of AV stenosis which is seen with CAVD.

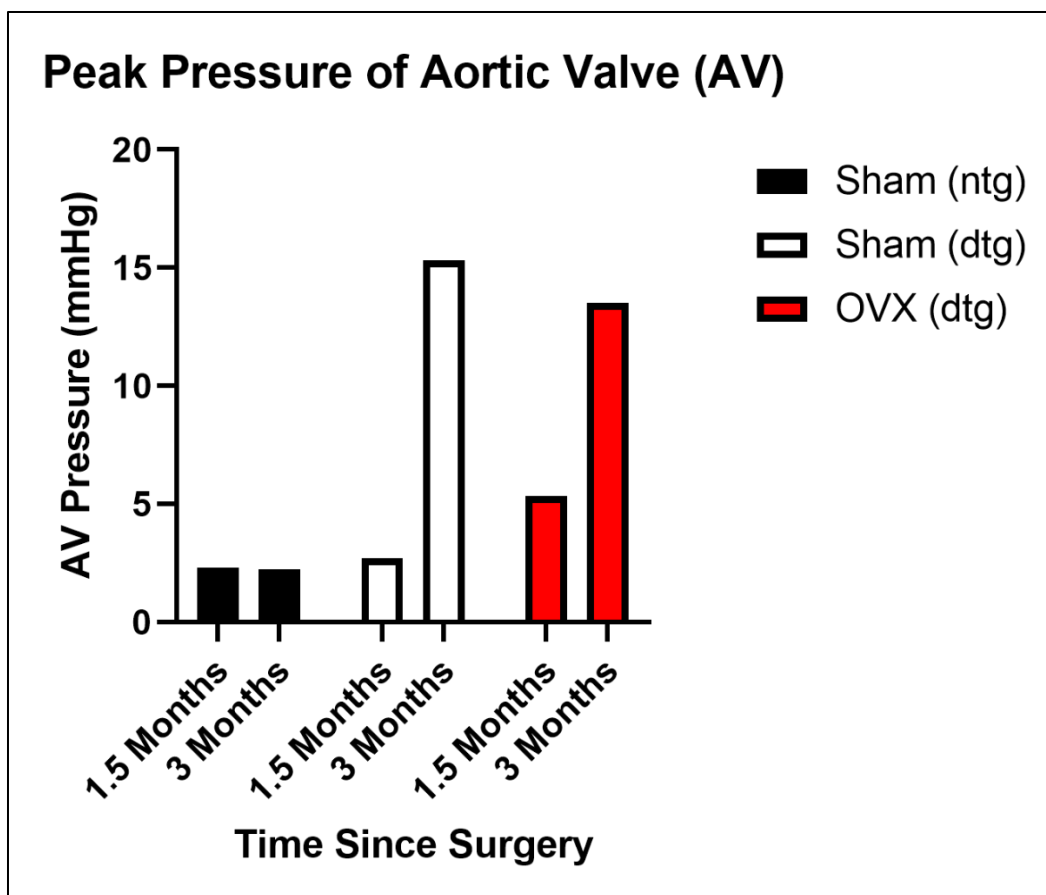


Figure 2.7 Changes in Peak AV Pressure of Mice in Preliminary OVX Study. Data on peak AV pressure was collected using a Vevo3100 with an MX transducer. The transducer was positioned in the Aortic Arch View (AAV) to acquire this data, and the data was processed using VEVO Analysis software provided by the Instrumentation Resource Facility at U of SC School of Medicine-Columbia. The x-axis shows when the data was collected on the mice, relative to time after surgery (either sham ovariectomy (OVX) or OVX). Also shown in the legend is whether the mouse is non-transgenic (ntg) or double transgenic (dtg). There is a clear increase in peak AV pressure in the mice that developed CAVD, however, the sample size was too small for all three groups (Sham ntg n=1, Sham dtg=1, OVX n=2) to do any tests of statistical significance.

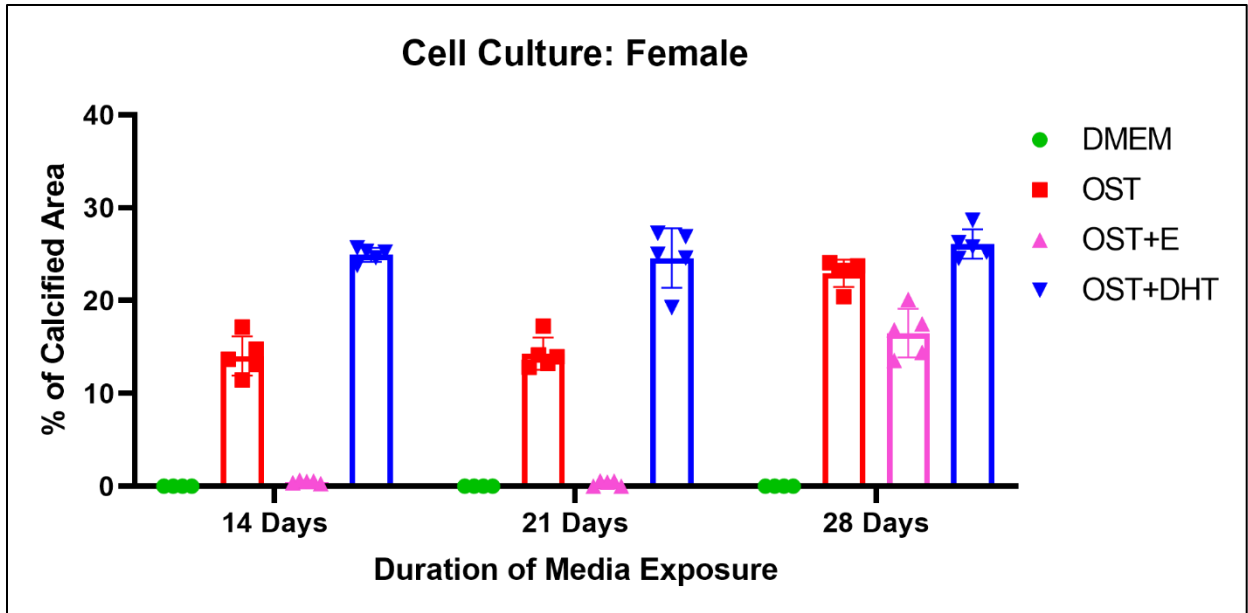


Figure 2.8 Quantification of Calcification of Female Murine VICs in Cell Culture. Cell cultures of female VICs were conducted in four 6-well plates. These cultures grew for either 14, 21, or 28 days. Once time expired, the cultures were processed for Alizarin red staining. Once staining was complete, photos (n=5 for each well) were taken of each of the four wells under a 4X microscope lens, and the % of calcified area was quantified using color threshold (threshold set at upper limit of 0 and lower limit of 115 for all) tool in ImageJ. This technique allows one to target and quantify the pixels associated only with calcified areas, as their color is unique relative to their surroundings. The colored bars are representative of the mean value of the 5 measurements for each condition and within these mean bars is the bidirectional standard deviation bar. A color coded legend is provided on the right hand side to indicate the type of media. Statistical significance cannot be determined as the experiment was only performed once.

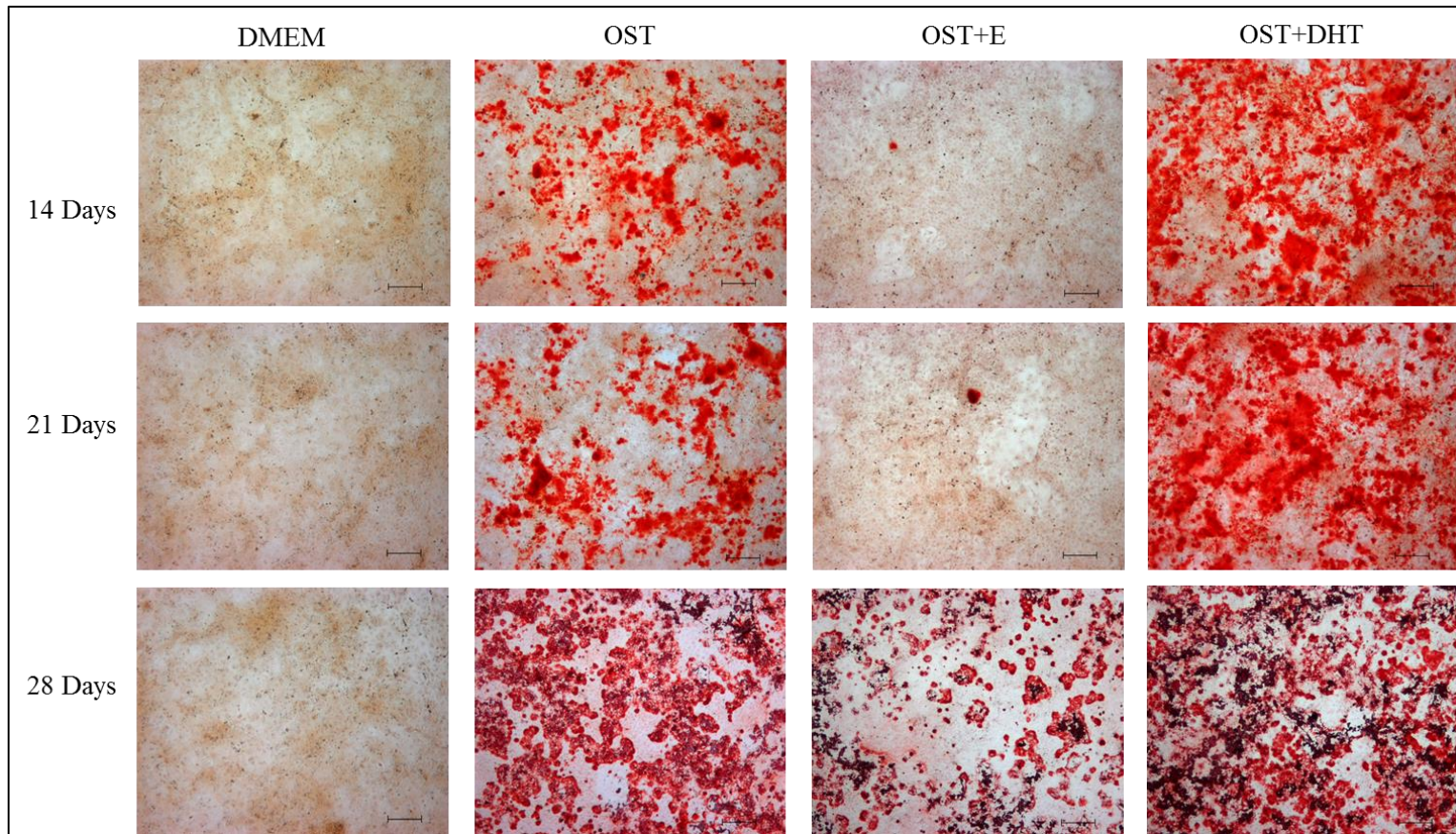


Figure 2.9 Representative Images of Wells in Female Cell Cultures. This figure gives a depiction of photos taken (n=5 for each well) of the wells using a Carl Zeiss camera at 4X magnification that were utilized for quantification of % of calcified area. In order left-to-right, the columns show DMEM, OST, OST+DHT, and OST+E media. The rows show 14 day, 21 day, and 28 day cell cultures in descending order. The scale bars are set 200 μ m.

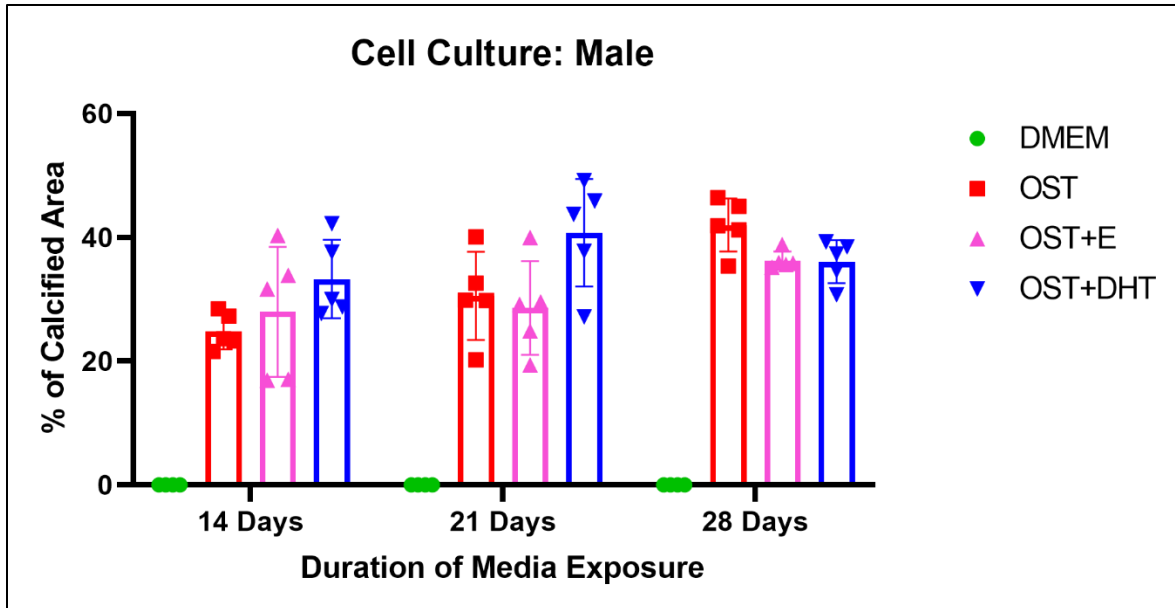


Figure 2.10 Quantification of Calcification of Male Murine VICs in Cell Culture. Cell cultures of male VICs were conducted in four 6-well plates. These cultures grew for either 14, 21, or 28 days. Once time expired, the cultures were processed for Alizarin red staining. Once staining was complete, photos (n=5 for each well) were taken of each of the four wells under a 4X microscope lens, and the % of calcified area was quantified using color threshold (threshold set at upper limit of 0 and lower limit of 115 for all) tool in ImageJ. This technique allows one to target and quantify the pixels associated only with calcified areas, as their color is unique relative to their surroundings. The colored bars are representative of the mean value of the 5 measurements for each condition and within these mean bars is the bidirectional standard deviation bar. A color coded legend is provided on the right hand side to indicate the type of media. Statistical significance cannot be determined as the experiment was only performed once.

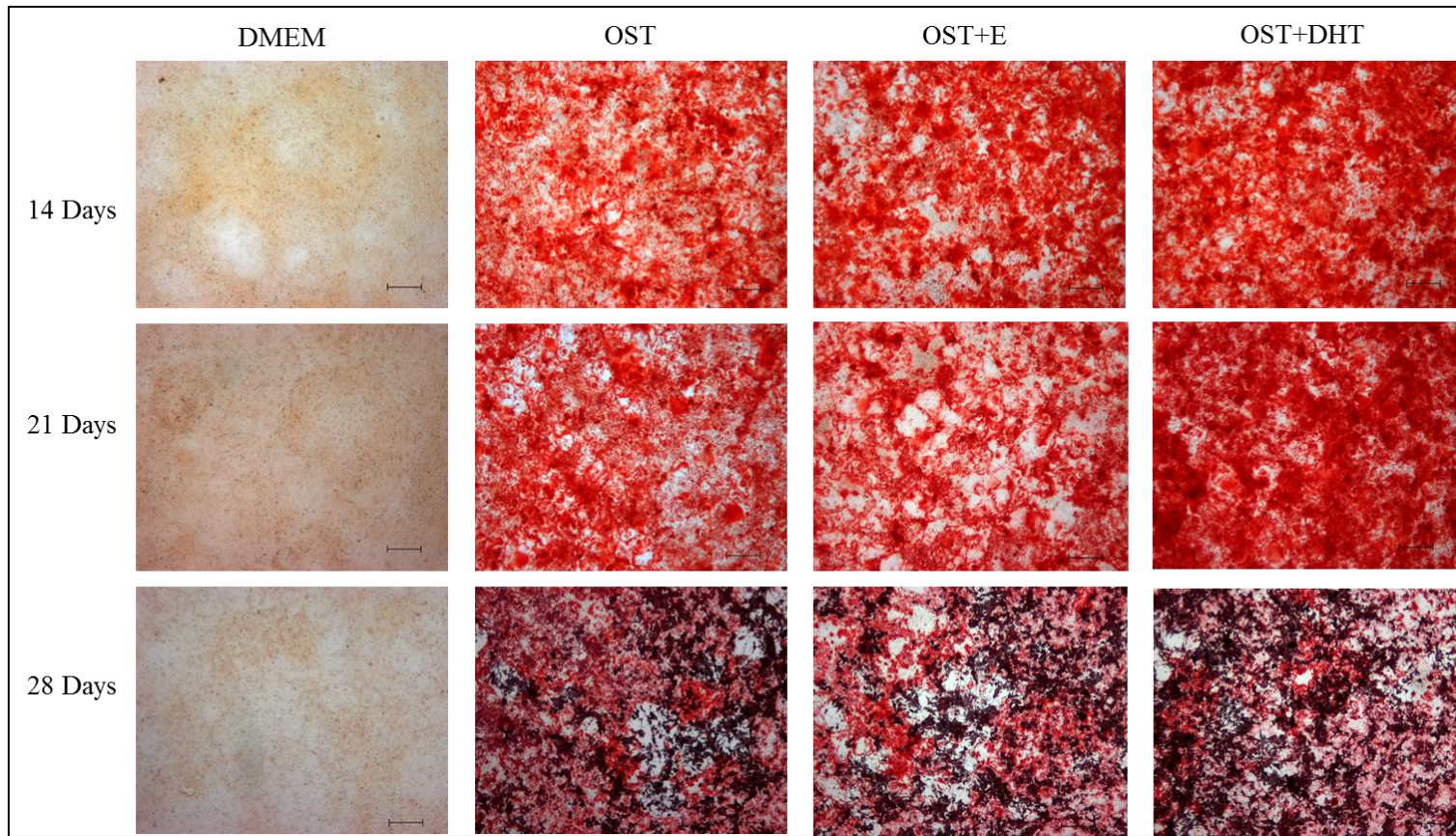


Figure 2.11 Representative Images of Wells in Male Cell Cultures. This figure gives a depiction of photos taken of the wells using a Carl Zeiss camera at 4X magnification that were utilized for quantification of % of calcified area. In order from left-to-right, the columns show DMEM, OST, OST+DHT, and OST+E media. The rows show 14 day, 21 day, and 28 day cell cultures in descending order. The scale bars are set 200 μ m.

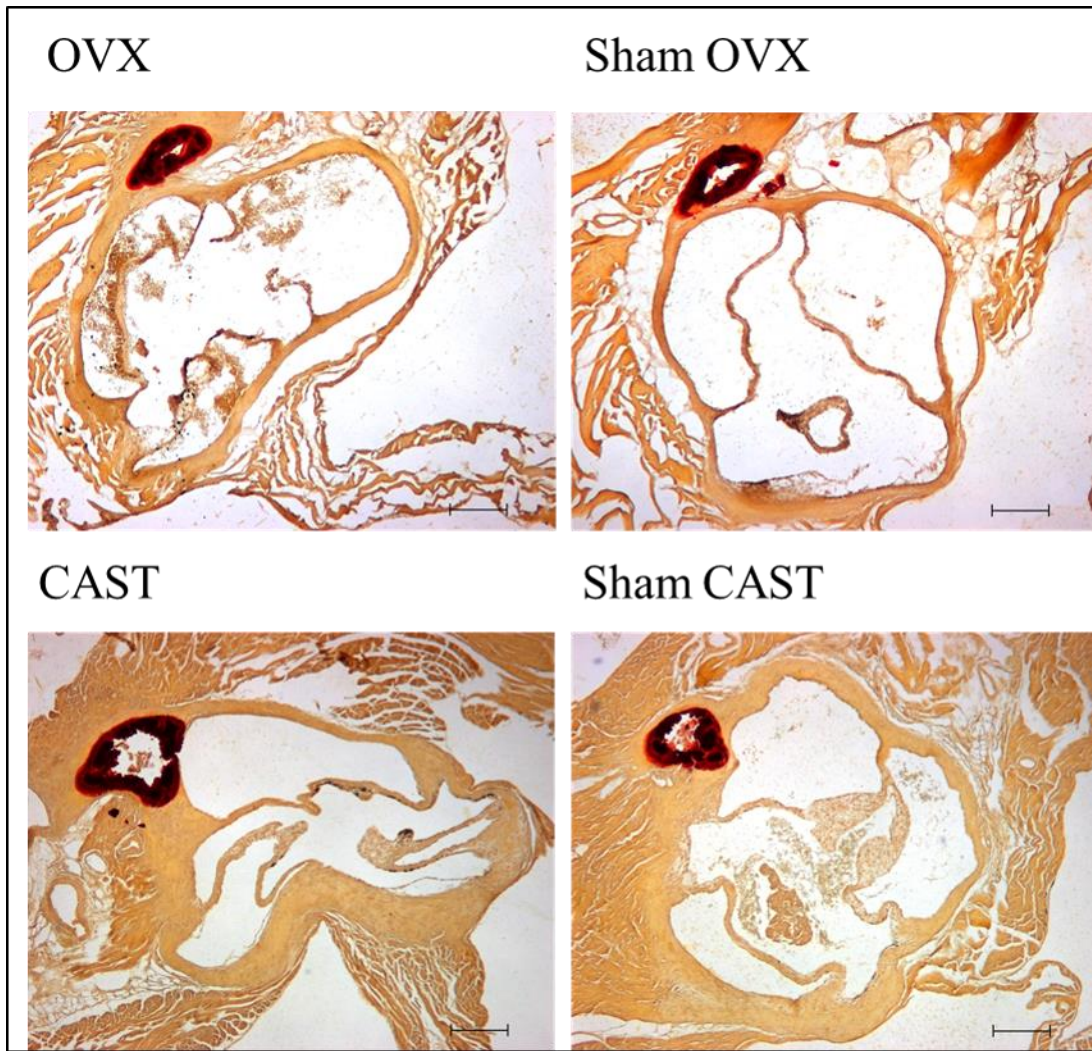


Figure 2.12 Alizarin Red Staining of AV from OVX & CAST Study. Alizarin Red Staining confirms the presence of calcification in and/or around the AV. All mice (n=11) developed calcification around the AV. These are representative images of that phenomenon. Each image was captured using a Carl Zeiss camera attached to a microscope in 4X magnification. Each image has a 200 μ m scale bar. Left-to-right, top-to-bottom: AV of OVX, AV of sham OVX, AV of CAST, and AV of sham CAST.

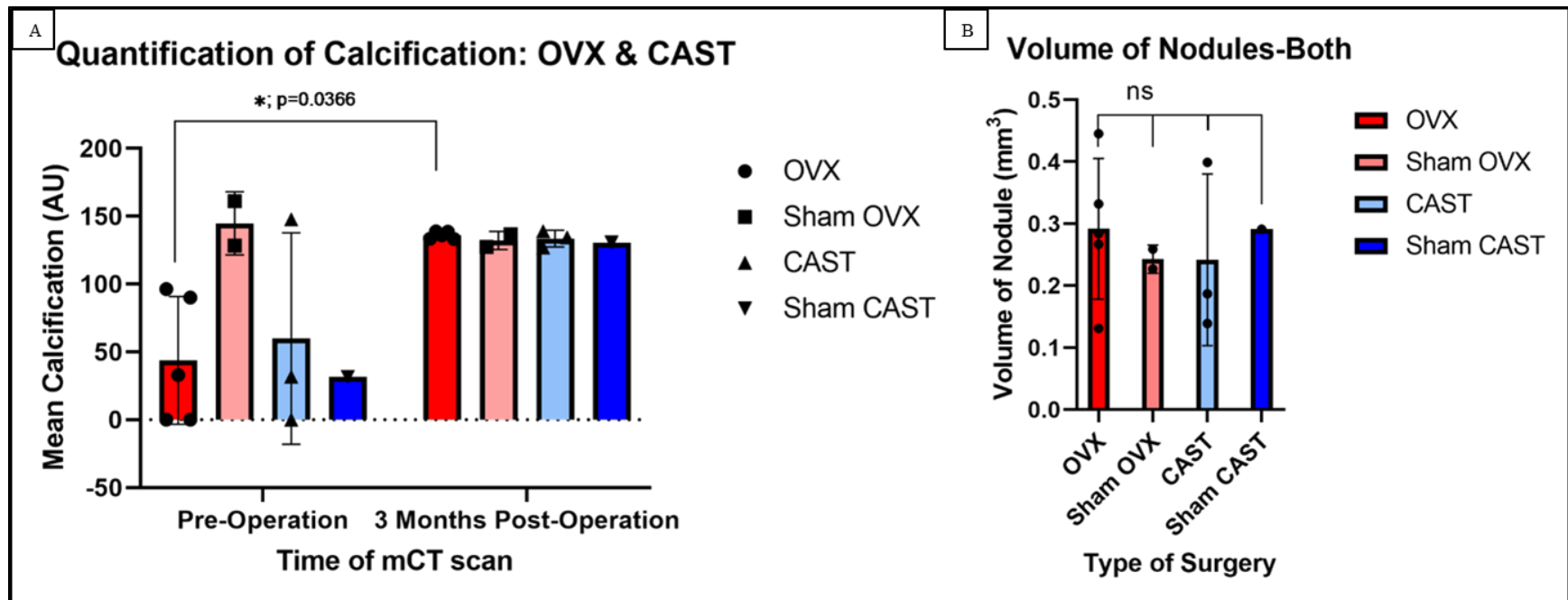


Figure 2.13 Quantification of Calcification and Volume Nodule in OVX & CAST Study. A) This graph shows the development of calcification from before surgery until three months later when the study was completed. The time of the scan being quantified is shown on the x-axis, and the y-axis shows the average ($n=5$ for each mouse) number of pixels detected (AU) for each mCT scan of each mouse in each group. This was quantified in ImageJ using color thresholding technique. B) This graph depicts the average volumes of the calcific nodules in mice ($n=11$) in each of the four groups at the end of the study. Each black dot within a group is associated with volume of the nodule in an individual mouse. The first bar represents the average volume of nodules in OVX, the second in sham OVX, the third in CAST, and the fourth in sham CAST. For both graphs, statistical significance was determined using a two-way ANOVA multiple comparisons with Tukey test. OVX=ovariectomy, sham OVX=no ovariectomy, CAST=castration, sham CAST=no castration

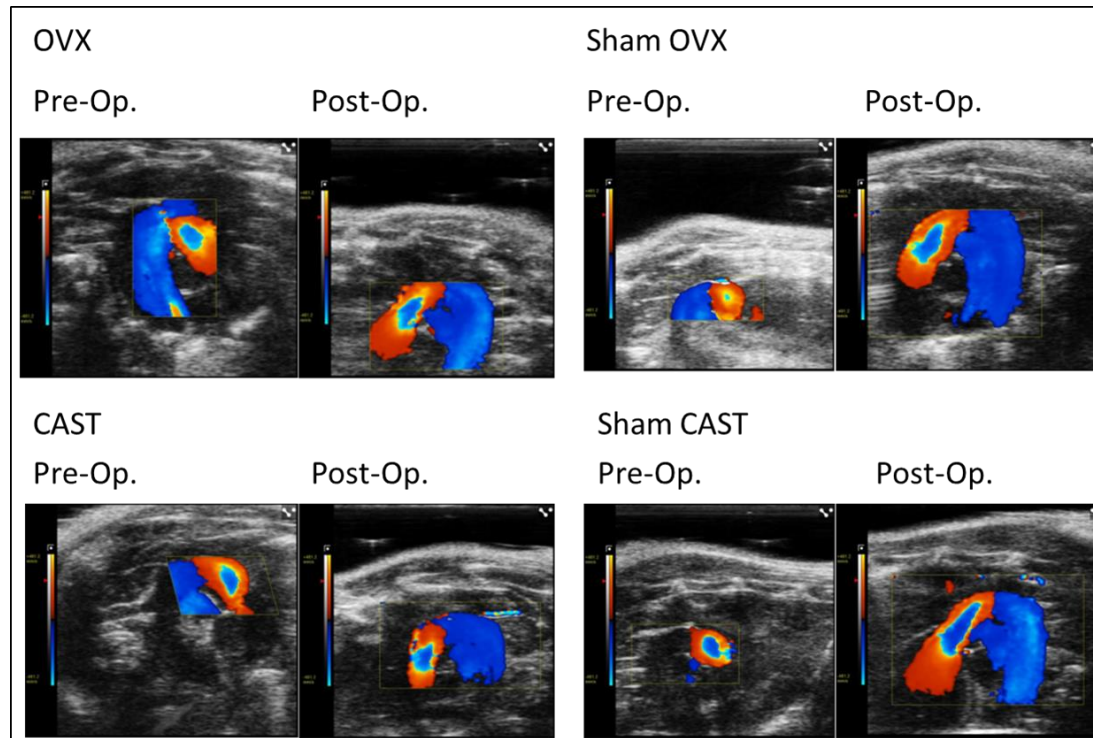


Figure 2.14 Doppler Imaging from OVX & CAST Project. These are representative images of the AVs of mice (n=11) captured using a Vevo3100 with an MX transducer. The transducer was positioned in the Aortic Arch View (AAV) to achieve a view of the aortic valve. Doppler imaging is a colorful visual representation of direction of blood flow. Red indicates that blood is flowing towards the transducer, while blue indicates that it is flowing away from the transducer. Every image above shows turbulence in movement of blood at the AV. This indicates there is constriction of blood flow at the AV. This is a classic diagnostic of AV stenosis seen in CAVD. The images (going left-to-right, top-to-bottom) show signs of AV stenosis in OVX, Sham OVX, CAST, and Sham CAST before and after surgery. OVX=ovariectomy, sham OVX=no ovariectomy, CAST=castration, sham CAST=no castration

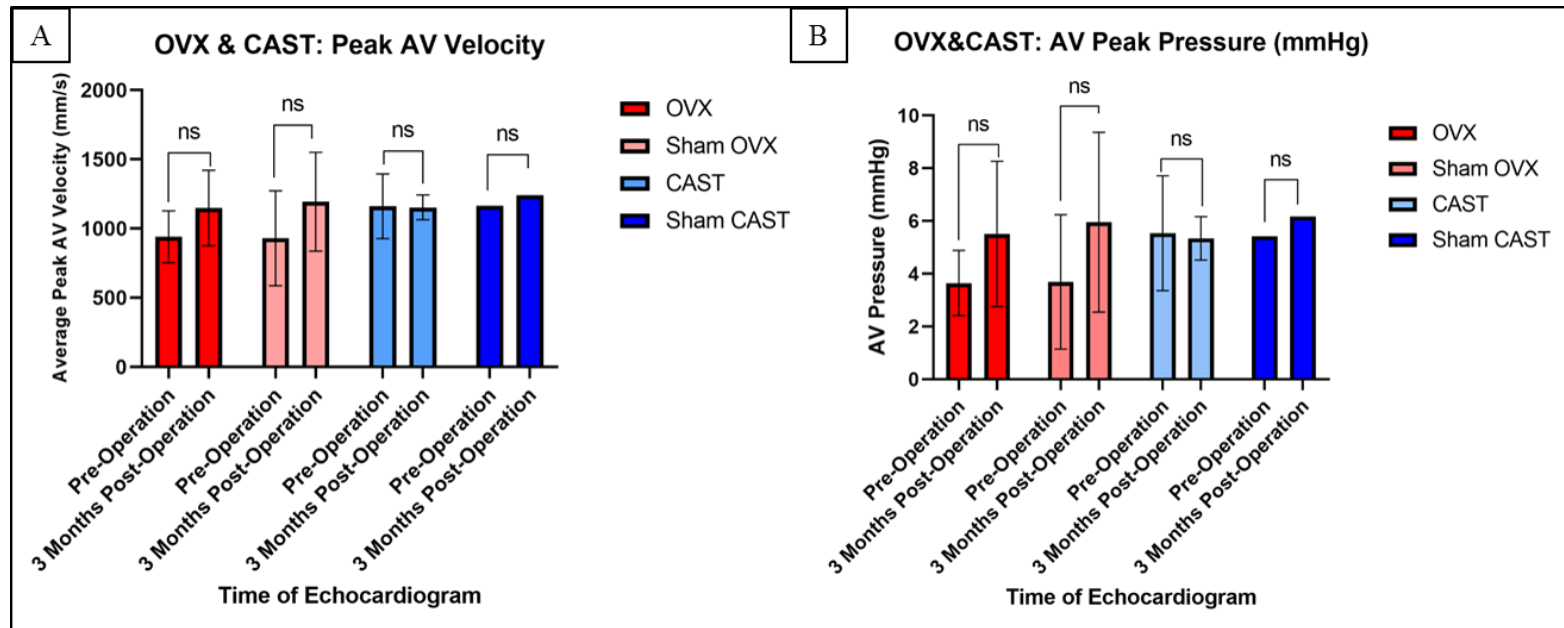


Figure 2.15 Initial and Final Peak AV Pressure in OVX & CAST Study. Data on peak AV pressure of mice (n=11) was collected using a Vevo3100 with an MX transducer. The transducer was positioned in the Aortic Arch View (AAV) to acquire this data, and the data was processed using VEVO Analysis software provided by the Instrumentation Resource Facility at U of SC School of Medicine-Columbia. The y-axis shows when the data was collected relative to surgery. Two-way ANOVA with multiple comparisons and a Tukey test indicated that there was no statistically significant change in the average peak AV pressure over the course of the study. OVX=ovariectomy, sham OVX=no ovariectomy, CAST=castration, sham CAST=no castration

CHAPTER 3

THE POTENTIAL OF EDTA AS A NON-INVASIVE TREATMENT OF CALCIFIC AORTIC VALVE DISEASE

Specific Aim 2: Determine if targeted delivery of EDTA using nanoparticles can be utilized as a non-invasive treatment for CAVD

3.1 Introduction

The chelating agent, ethylenediamine tetra acetic acid (EDTA), offers promising potential as a means of removing calcification in cardiac tissue (Clarke et al., 1955; Nosoudi et al., 2016). EDTA interrupts divalent calcium bonds (Ca^{2+}) by splitting the calcium ions apart and isolating an individual calcium ion within the EDTA molecule where it forms a stable bond; this then leads to a reduction in calcification of cardiac tissue and removal of these excess ions via the urinary tract (Nosoudi et al., 2016; Cranton, 2001). Chelation therapy targeting cardiovascular ailments first occurred in 1955 when Clarke et al., experimented with its ability to treat atherosclerosis. Based on their positive results, as well as others, the use of EDTA chelation therapy has continued to become more prevalent. There was a 68% increase (from 66,000 to 111,000) in EDTA chelation therapy used in treatment for adults from 2002 to 2007 (Barnes et al., 2008).

EDTA chelation therapy is controversial due to harmful side effects. EDTA will react with calcium deposits in cardiac tissue, but it will also react with calcium throughout the body. EDTA forms bonds with calcium ions in the serum and can cause bone loss and hypocalcemia (Seely et al., 2005). This is a primary reason why the FDA has not approved chelation therapy (Lei et al., 2014). Nanoparticle (NP) technology offers a way to circumvent this limitation of chelation therapy.

NPs allow for the targeted delivery of EDTA to the sites of calcification. The composition of NPs varies and a number of modifications can be made on them so that they can interact with specific targets and/or locations. They can be composed of poly(lactic acid), poly-cyanoacrylate, or poly(D,L glycolide) among many other things (Pitt et al., 1981). The NPs used in this research project were albumin nanoparticles that were coated with elastin antibodies (Figure 3.1) (Lei et al., 2014). These antibodies specifically target damaged elastin. They were designed this way because a recurrent phenomenon observed in vascular diseases is the degradation and fragmentation of elastic lamina (Sinha et al., 2014). The elastin fibers of the aorta are normally covered with microfibrillar glycoproteins like fibulins and fibrillins, but, in cases of vascular and valvular calcification, the microfibrillar glycoprotein coat around the elastin core has worn away (Figure 3.2) (Sakai et al., 1986; Pai & Giachelli, 2010; Rosenbloom et al., 1993; Sinha et al., 2014). The NPs will only target and bind to the damaged portions of the elastin fibers around the elastic lamina, close to the areas of calcification, where they will then release the EDTA.

The ability of NP-delivered EDTA to reverse CAVD needs to be researched as there is little to no research on chelation therapy that specifically targets calcification of the aortic valve. Specific, targeted delivery of EDTA to sites of calcification could lead to significant improvements in quality of life for patients suffering from CAVD. In the past, EDTA has showed potential as a treatment for calcification. However, the negative side effects have prevented it from becoming a mainstream treatment. Targeted delivery of EDTA using NPs provides an alternative, non-invasive treatment that would spare patients from risky surgical procedures that only provide a short term solution. This

project focused on using elastin-antibody labeled albumin NPs as a treatment to reduce calcification of the AV. The hypothesis is that treatment of mice with CAVD using elastin-antibody labeled albumin NPs will lead to reduced calcification in the AV and improvements in heart function.

3.2 Materials and Methods

3.2.1 Mice

All animal work was performed in accordance to protocol approved by the Institutional Animal Care and Use Committee (IACUC) at University of South Carolina. All mice were available in the Azhar laboratory. The mice used in this study were TGF β 1 transgenic (Tg), Postn-Cre Tg, or Postn-Cre non-transgenic (nTg). All mice in this study were at least 1 year old.

3.2.2 microCT Imaging

microCT (mCT) scans of mice in this project allowed for imaging and tracking of the level of calcification in the aortic valve, as well as other cardiac tissue. First, the Perkin Elmer Quantum GX machine was turned on and allowed to warm up for 15 minutes. Once this was done, 1.5-2% isoflurane was added to its appropriate containment and regulatory chamber, the oxygen supply was turned on, the vacuum pump system initiated, and the anesthesia muzzle was properly placed on the apparatus that holds the mice during the scan.

The mice were anesthetized in a box that circulated a mixture of oxygen and isoflurane. Once the mouse was anesthetized, it was quickly moved from this box into the Quantum GX. The mouse was then placed in a supine position, with its snout inserted carefully into the anesthesia muzzle. The Quantum GX door was then closed and the scan was started. All scans were done with the following settings: field of view (FOV) set to

FOV45, High Resolution, 4 minute scan, X-ray filter of Cu 0.06+ Al 0.5. Once the scan was finished, anesthesia was stopped and the mouse was moved to a recovery cage. The images were saved and collected.

3.2.3 Echocardiography

Heart and valve function of the mice was tracked using echocardiography. A Vevo3100 with an MX400 transducer was the instrument used to achieve this. The transducer was positioned to achieve three primary views of the heart: Aortic Arch View (AAV), Parasternal Long Axis (PLAX) View, and Parasternal Short Axis (PSAX) View. To get the desired views of the heart, the *Guide to Small Animal Echocardiography using the Vevo® 2100 Imaging System* published by VisualSonics was followed.

Before imaging of the heart could be done, the mice were anesthetized in a box that circulated a mixture of oxygen and isoflurane. Once the mouse was anesthetized, protective lubricant was placed over its eyes, and then the mouse was laid on the imaging platform and had its snout placed into the anesthetizing tube. Once there, its hands and feet were placed onto the sensors that tracked heart and breathing rate and fastened down with tape. Heart rate was maintained about 400 beats per minute. The mouse's hair was removed from its chest and upper abdomen using Nair. Once the hair and Nair were appropriately washed away, gel was placed onto the transducer and imaging could begin.

To acquire the PLAX and PSAX View, the imaging platform the mouse was on was tilted down slightly. The transducer was placed such that the notch on the transducer was pointing towards the mouse's head and the rotated approximately 35° counter clockwise. From this view data could be collected for PLAX. To transition from

collecting data in the PLAX view to the PSAX view, the transducer was rotated 90° clockwise from the PLAX View. In these two views, M-Mode data was collected.

To acquire data relating to the aortic valve function, the right side of the imaging stage was tilted down, and the transducer was placed on the left side of the mouse such that the notch was pointing towards the mouse's head and was parallel with the chest. The transducer was moved and angled until a good view of the aortic arch was achieved. The innominate, subclavian, and left common carotid arteries served as landmarks to help achieve this view. In this view data relating to blood flow was collected using Color Doppler and PW Doppler.

Four key categories of left ventricular function were measured: fractional shortening, ejection fraction, stroke volume, and cardiac output. Respectively, the normal values for these measurements in mice are 30-50%, 55-85%, 40-70 μ L, and 20-35 mL/min. These measurements were provided in the *Guide to Small Animal Echocardiography using the Vevo® 2100 Imaging System* published by VisualSonics.

3.2.4 EDTA-Nanoparticles Injections

Doctoral candidate, Mengistu Gebere, prepared and performed all EDTA-nanoparticle injections of the mice. The nanoparticles were prepared at Dr. Vyavahare's lab. To prepare them, 4 μ L of distilled deionized water were used to dissolve 100 mg of EDTA and 200 mg bovine serum albumin. 6 N NaOH was used to adjust pH of this solution until it reached a pH of 8.5. Drop-wise addition of the solution into 16 mL of ethanol was conducted for probe sonication. Probe sonication was done for 1 hour. Glutaraldehyde, at a concentration of 10 μ g per mg of BSA, was added during sonication to achieve crosslinking. (Karamched et al., 2019).

To conjugate the elastin antibodies to the nanoparticles, 34 μg of Traut reagent was used for thiolation of 10 μg of rabbit anti-rat elastin antibodies. This solution was then added to 4-(2-hydroxyethyl)-1-piperazineethanesulfonic acid (HEPES) buffer (20 mmol/L; pH of 9.0) where it incubated at room temperature for an hour. The antibodies were then rinsed with HEPES buffer, added to the nanoparticles (4 μg per 1 mg nanoparticle), and incubated overnight to allow for conjugation. The conjugated nanoparticles and antibodies were twice washed with PBS, and then centrifuged at 10,000 revolutions per minute for 10 minutes. Finally, they were suspended in 0.03% rat serum albumin (Nosoudi et al., 2015).

The injections were done into the tail vein of the mice twice a week at a concentration of 10 mg/kg (based on the body weight of a mouse). The EDTA NPs were received in a powdered form. This powder was dissolved in 1X PBS to achieve the concentration of 10 mg/kg for each tail vein injection.

3.2.5 Tissue Collection and Processing

At the end of the studies, mice were sacrificed by being placed in a chamber containing isoflurane. Once deceased, its heart was retrieved from the body and placed in a vial containing 4% paraformaldehyde for 24-48 hours. The heart was then held in 70%, 95%, and 100% ethanol for 24 hours each. After this, the vial containing the heart was filled with xylene and placed in a vacuum oven at 60 °C for three hours. This was done twice with a change into new xylene for the second three hour period. After that, the heart was left overnight in a 50% xylene, 50% paraffin mixture. The next day, the xylene-paraffin mixture was melted, removed, and replaced with 100% paraffin in the vial. The vial was then be placed in the vacuum oven at 60 °C for 4 hours. After 4 hours, the vial

was removed from the oven and the heart was held overnight in this paraffin. The next day, the vial was placed into the vacuum oven at 60 °C for two 4 hour periods, with a change of paraffin before the second period. Once this was done, the heart was placed into a mold and was ready to be sectioned, placed on microscope slides, and exposed to various histological staining.

3.2.6 Alizarin Red, Alcian Blue and von Kossa, Hematoxylin-Eosin-Y Staining

Before any of the microscope slides with tissue sections could be stained, they first had to be deparaffinized in three washes of xylene for 3 minutes each. The tissue was then hydrated. To achieve this, slides were placed in two washes of 100% ethanol for 2 minutes each, then in 95% ethanol for a minute, 70% ethanol for a minute, and then were gently washed in deionized water for approximately a minute.

Next, for Alizarin Red Staining, Alizarin Red solution was placed directly onto the tissue sections using a pipette to carefully add drops of the staining solution until it covered the section. The staining solution stayed on the section for 5 minutes. After 5 minutes, the Alizarin Red solution was completely removed from the tissue section. The slide was then placed in acetone for 1 minute, and then a 50/50 mixture of acetone and xylene for 15 seconds. The slide was then cleared in three changes of xylene for three minutes in each change. Finally, the slide was air dried and a coverslip with permanent mounting media was placed over the tissue section.

For Alcian Blue and von Kossa staining, once the slides had been deparaffinized and hydrated in water, they were then moved into a clear, plastic cassette that contains 1% silver nitrate. The cassette was then placed under ultraviolet light for an hour. After an hour had passed, the silver nitrate was removed from the cassette and the slides were

washed with deionized water for approximately a minute. The cassette with the slides was then filled with 5% sodium thiosulfate for 5 minutes to remove any un-reacted silver. After these 5 minutes, the slides were washed in deionized water for approximately one minute. The cassette was then filled with Alcian Blue staining solution. The slides were held in this for 30 minutes. Next, the Alcian Blue is removed and the slides were washed with deionized water until all the excess Alcian Blue had been removed. The cassette with the slides was then filled with nuclear fast red counterstain for 5 minutes. After this, the nuclear fast red was removed and the slides were washed in deionized water. The slides were then dehydrated in one wash of 70% ethanol, one wash 95% ethanol, and finally three washes of 100% ethanol for a minute each. The slides then went through three washes of xylene, each of which lasted for three minutes. Finally, the slides were air dried and a coverslip was permanently mounted over the tissue section.

For Hematoxylin-Eosin-Y staining, the slides were placed in ANATECH Hematoxylin (Normal Strength) for 7 minutes. After this, they were gently washed in deionized water for a minute. Next, the slides were submerged in acid alcohol (95% ethanol, 10% acetic acid) for a minute and then 1% sodium bicarbonate (bluing reagent) for 1 minute, with a 1 minute deionized water rinse in-between exposure to the two solutions and after the bluing reagent step. The slides were then in 70% ethanol for 2 minutes before being placed into ANATECH Eosin-Y for 2 minutes. The slides were then dehydrated in one wash of 70% ethanol, one wash 95% ethanol, and finally three washes of 100% ethanol for a minute each. The slides then went through three washes of xylene, each of which lasts for three minutes. Finally, the slides were air dried and a coverslip was permanently mounted over the tissue section.

3.2.8 Quantification and Statistical Analysis of Data Collected

Color thresholding in the NIH software, ImageJ, allows one to quantify calcification within a live mouse based on imaging collected from mCT scans. This is achieved when pixels of an individual image within a stack of hundreds of images (collected during a scan) are counted using an interactive image-altering technique called, Color Threshold. The calcified nodule will appear white, similar to bone, in a normal mCT image. To quantify the presence of calcification, one must change the color threshold settings until bone-like material, but not tissue, appear red. This indicates that pixels are being tagged onto bone-like material. Those pixels can then be counted. Once the nodule is located, one can set parameters to measure specifically in the area around the nodule and begin quantifying the level of calcification. Measurements are taken for as much of the calcified area as possible where pixels are being tagged to the calcification.

Quantification of ECHO data was done using FujiFilms VEVO Analysis software provided by the Instrument Resource Facility at U of SC School of Medicine-Columbia. Statistical analysis was conducted in GraphPad Prism 9. Specifically, one-tailed paired t-test and two-tailed paired t-test to determine statistical significance before and after EDTA-NP treatment.

3.3 Results

3.3.1 EDTA Treatment Reduces Calcification of the Aortic Valve

Alizarin Red and von Kossa staining confirmed the presence of the calcific nodules in the tissue of the aortic root (AR) (including the aortic valve (AV)) (Figure 3.3). Alcian Blue staining confirmed the proteoglycan precursor state that gives way to further calcification (Figure 3.3).

EDTA injections significantly reduced the calcification of the AV in all mice (n=5) that received the treatment, regardless of how many injections they received (Figure 3.5). This does not include the mouse that only received one injection of EDTA (Figure 3.5). This phenomenon was quantified using color thresholding on ImageJ.

Significant (p=0.0043) reduction of calcification in the AV was also confirmed by calculating the volume of the calcified nodules seen in microCT (mCT) scans (Figure 3.4). The average initial size of the nodules before EDTA treatment was approximately 2 mm³. After EDTA treatment, the average size of the calcified nodule was reduced to less than 1 mm³ (Figure 3.6).

3.3.2 No Significant Change in Left Ventricular Function

Insights into AV function can be assessed by determining the health of the left ventricle (LV), as the two are inextricably connected. LV function was assessed by taking M-mode measurements using echocardiography. The dimensions and volume of the LV are measured and several metrics are acquired from this. Four key categories measured are fractional shortening, ejection fraction, stroke volume, and cardiac output. Respectively, the normal values for these measurements in mice are 30-50%, 55-85%, 40-70 μ L, and 20-35 mL/min. Results from data collected from the mice (n=5) before and after treatment using EDTA nanoparticles showed no statically significant improvement in any of the four categories of LV function after treatment (Figure 3.7). Relative to what are the agreed upon normal values, these mice were, on average, in the normal range for ejection fraction and fractional shortening. The average ejection fraction was 73.88% before treatment and 66.87% after treatment. The average fractional shortening was 45.06% before treatment and 37.75% after treatment. The mice were

below normal threshold for cardiac output and stroke volume. Before treatment, the average cardiac output was 16.24 mL/min and after treatment it was 15.34 mL/min. Stroke volume was 35.45 μ L before treatment and 31.60 μ L after.

3.4 Discussion

The focus of this study was to determine the viability of targeted elastin-antibody labeled albumin nanoparticles (NPs) infused with ethylene diamine tetraacetic acid (EDTA) as a non-invasive treatment for calcific aortic valve disease (CAVD). The results show this treatment to be effective in removing calcification in and around the aortic valve (AV). Our genetic mouse model using TGF β 1/PeriCre mice proved to be appropriate for this study. The development and progression of CAVD was tracked and confirmed using microCT (mCT) scans. Additionally, histological staining designed to determine the presence of calcification in tissue further confirmed calcification localized to the aortic root (AR), which the AV is a part of. This study showed that total calcification and volume of the calcific nodule was significantly reduced in all mice that received multiple injections of EDTA NPs. This treatment did not, however, show to have any statistically relevant impact on improving heart function of the mice.

The efficacy and safety of chelation therapy as a treatment for removing atherosclerotic plaques is still a controversial topic. The FDA has still not approved its use as a treatment for diseases relating to this condition. The primary reason for skepticism of chelation therapy is that the treatment will not only target malignant plaques, but also react with calcium in plasma and bones. Additionally, there is great debate in terms of which chelating agent would be best to use in such a therapy. The key to making chelation therapy a viable treatment is to determine which chelating agent is the most effective and to deliver this agent specifically to malignant plaques. Previous

research compared three chelating agents, EDTA, diethylene triamine pentaacetic acid (DTPA), and sodium thiosulfate (SDS), to determine which was the best chelating agent to treat sclerosis of the medial vascular tissue of the aorta and found that EDTA was the most effective (Lei et al., 2013). This study also used elastin-specific NPs and found that systemic calcium levels and vascular structure were not compromised (Lei et al., 2013). Another study showed similar results using elastin-specific EDTA-loaded albumin NPs to treat medial arterial calcification (Lei et al., 2014). One interesting difference is that this study claims to have seen complete removal of arterial calcification in 4 of the 5 arteries after just four injections (2 weeks) (Lei et al., 2014). Our project used the same NPs and injection concentrations, but we did not observe complete removal of calcification. Only a reduction in calcification. This could be due to a difference in the disease being studied. It may be more difficult to remove calcification in the AV and require more injections to achieve complete eradication of calcification.

To our knowledge, this is the first study to specifically study the use of elastin-antibody labeled albumin NPs infused with EDTA to treat CAVD. Our findings suggest that this treatment method is effective at reducing the calcification of the AV, however it is unclear whether this improves heart function. Further research needs to be done to confirm these findings. This study had a limited number of mice (n=5) that received multiple injections. The echocardiography data does not look promising, but it was collected in the early stages of my use of the VEVO3100. Additionally, data specific to the AV was not effectively collected. Only data relating to LV function. A more experienced researcher may have collected more promising data. There also needs to be more research into how many injections it may take to completely remove the

calcification of the AV, as well as studies on the effects of this treatment on AV structure. Ultimately, our hypothesis that EDTA-infused elastin-antibody labeled NPs could reduce calcification of the AV proved correct, however there can be no such conclusions in terms of whether heart function was improved.

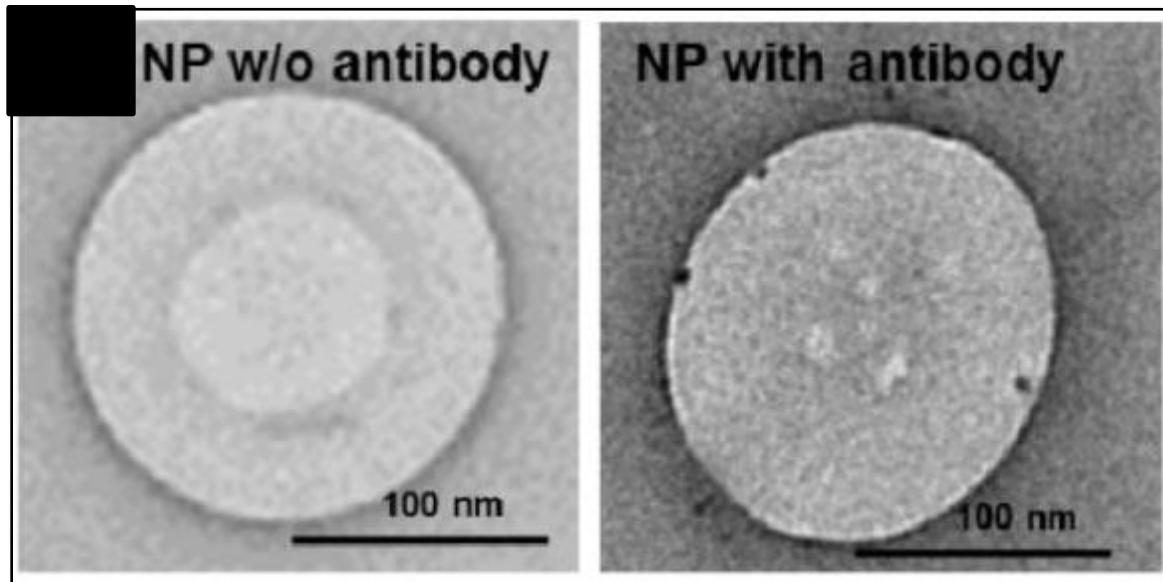


Figure 3.1 Structure of Albumin Nanoparticle. This is a visual representation of albumin nanoparticles with and without antibodies on it. The nanoparticle on the right side of the image possesses IgG antibodies. This figure has 100 μm scale bars. This figure was taken from Lei et al., 2014. Permission to use this image was granted by Elsevier to reproduce the aforementioned material subject to the terms and conditions indicated.

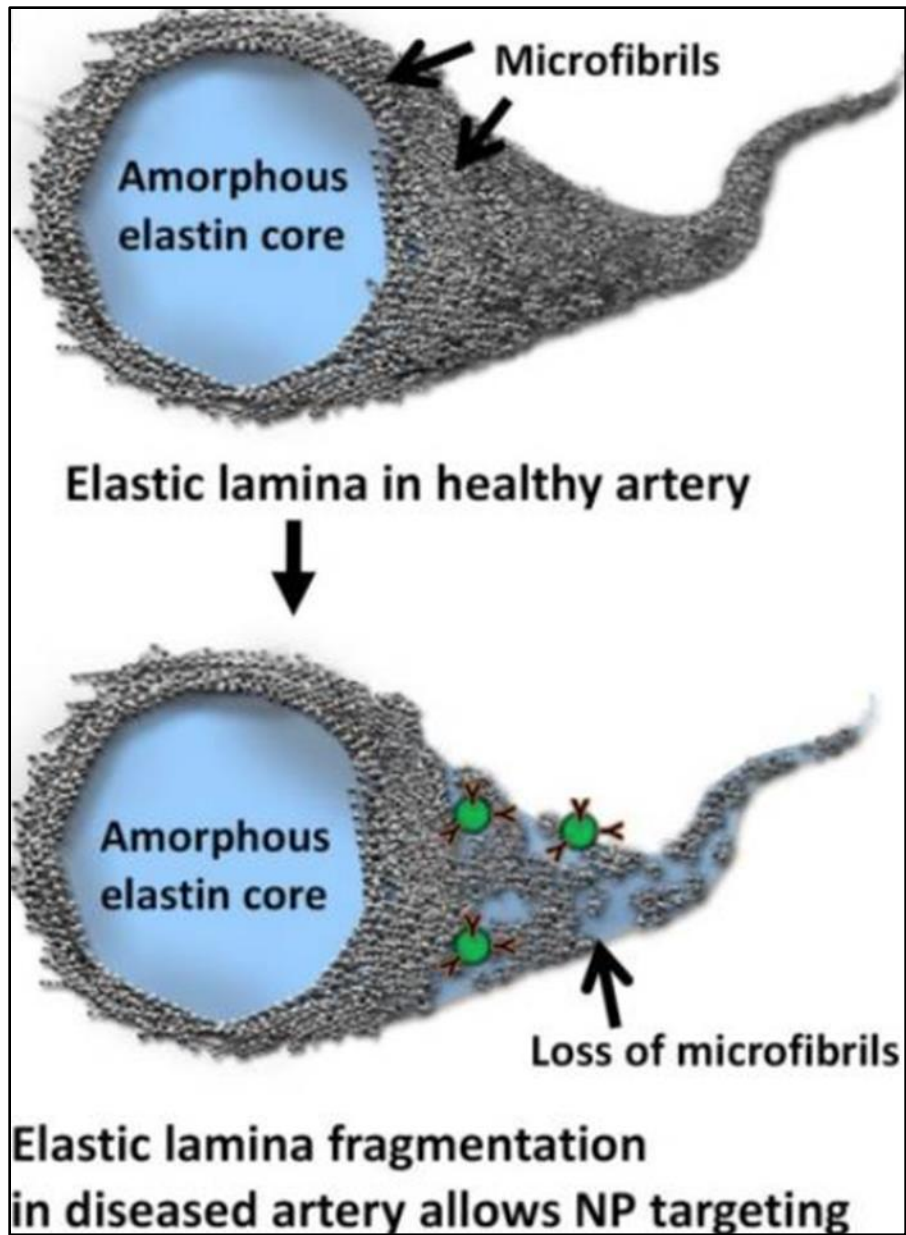


Figure 3.2 Comparison of Healthy vs Damaged Elastin Fibers. This image is a representation of the difference between an intact elastin fiber in a healthy artery and a damaged elastin fiber that has had its microfibrils worn away. The nanoparticles are specifically designed to target the damaged elastic lamina, as is shown in the bottom portion of the image. This figure was taken from Sinha et al., 2014. Permission to use this image was granted by Elsevier to reproduce the aforementioned material subject to the terms and conditions indicated.

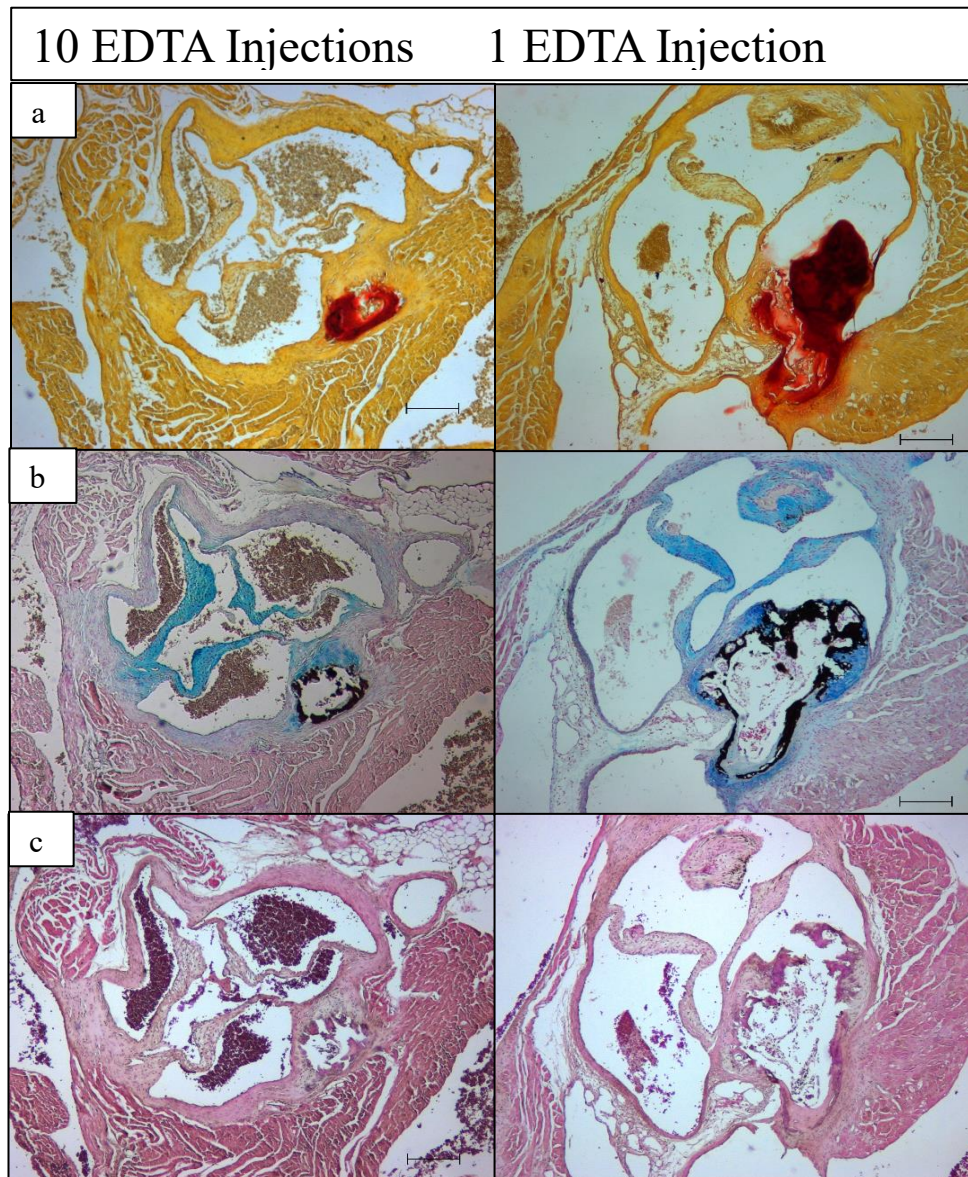


Figure 3.3 Histological Staining of Aortic Valve After Targeted EDTA Treatment. All of these images were captured using a Carl Zeiss camera on a microscope in 4X magnification. Each image has a 200 μm scale bar. a) Alizarin Red Staining confirms the presence of calcification in and/or around the AV. Areas of calcification stain red when exposed to Alizarin Red staining. b) Alcian Blue and von Kossa staining provide more context around the sites of calcification. Alcian Blue staining stains proteoglycans which are a precursor state to calcification. Tissue that is stained blue is likely more rigid and more prone to calcify relative to non-stained tissue. von Koss staining further confirms presence of calcification by staining calcified sites black. c) Hematoxylin-Eosin-Y staining shows nuclei and cytoplasmic components. Of note in this image, areas that are a lighter, whitish color are composed of cartilaginous tissue.

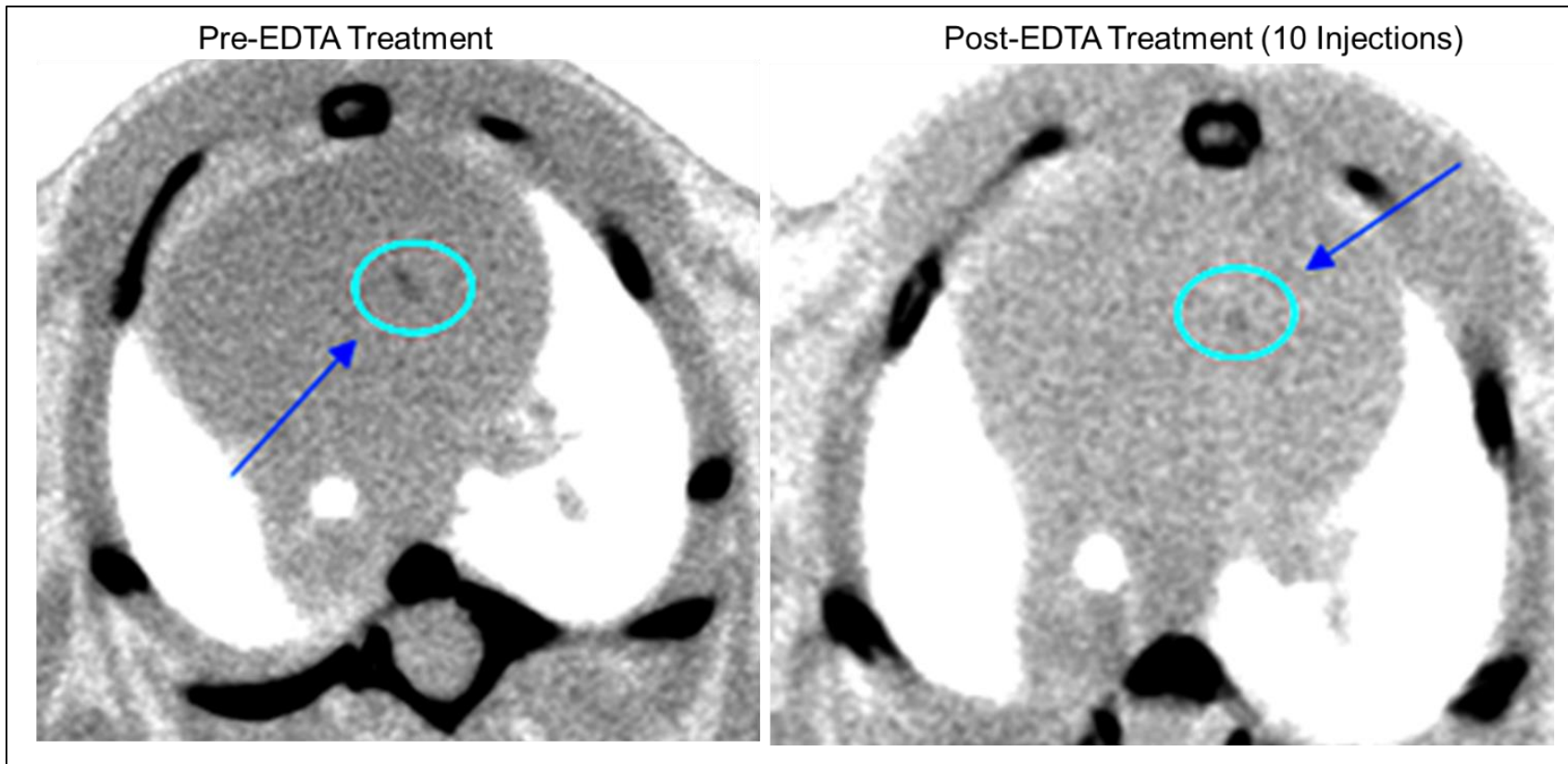


Figure 3.4 microCT of Aortic Valve Before and After Targeted EDTA Treatment. This is a representative image of the reduction of a calcified nodule in a mouse's heart before and after targeted EDTA treatment. The calcified nodule is circled in turquoise with a blue arrow pointing to it. These images are in approximately the same XZ-axis location in the same mouse and were collected in 4-minute, FOV45 scans using Perkin Elmer Quantum GX.

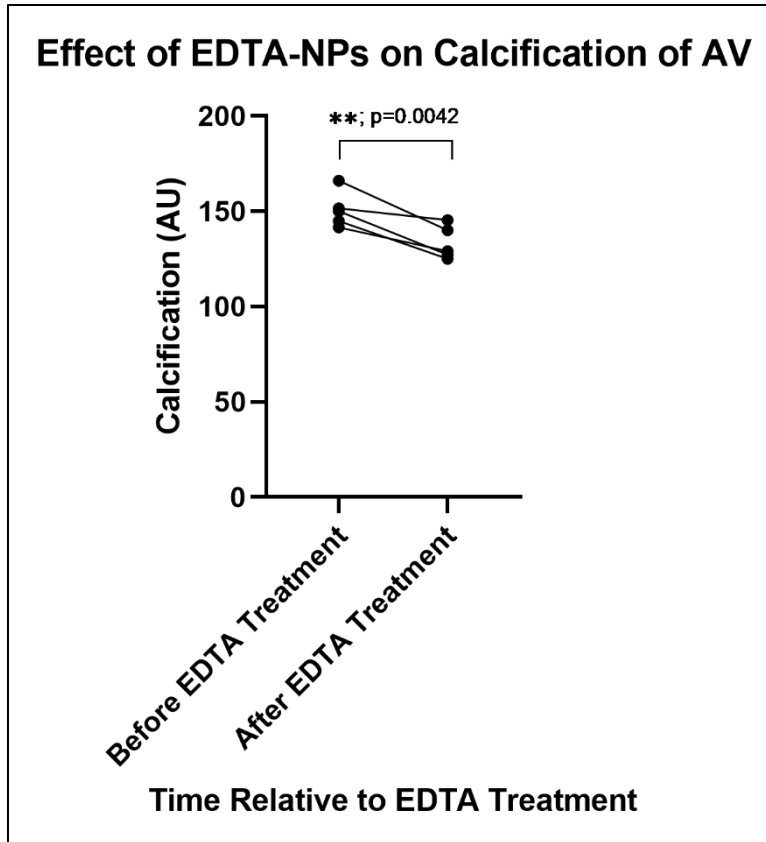


Figure 3.5 Quantification of Reduced Calcification. This image shows the average calcification present in the AV of mice (n=5) before and after targeted EDTA treatment determined via color thresholding of mCT scans. The time of the mCT scan is shown on the x-axis, and the y-axis shows the average number of pixels detected (AU) from a scan for each mouse (represented by a dot). Above the mean values for each mouse group is a symbol denoting the statistical significance (**; p=0.0042) between the average initial and final measurements of the study. Statistical significance between the initial and final values was determined using a one-tailed paired t-test.

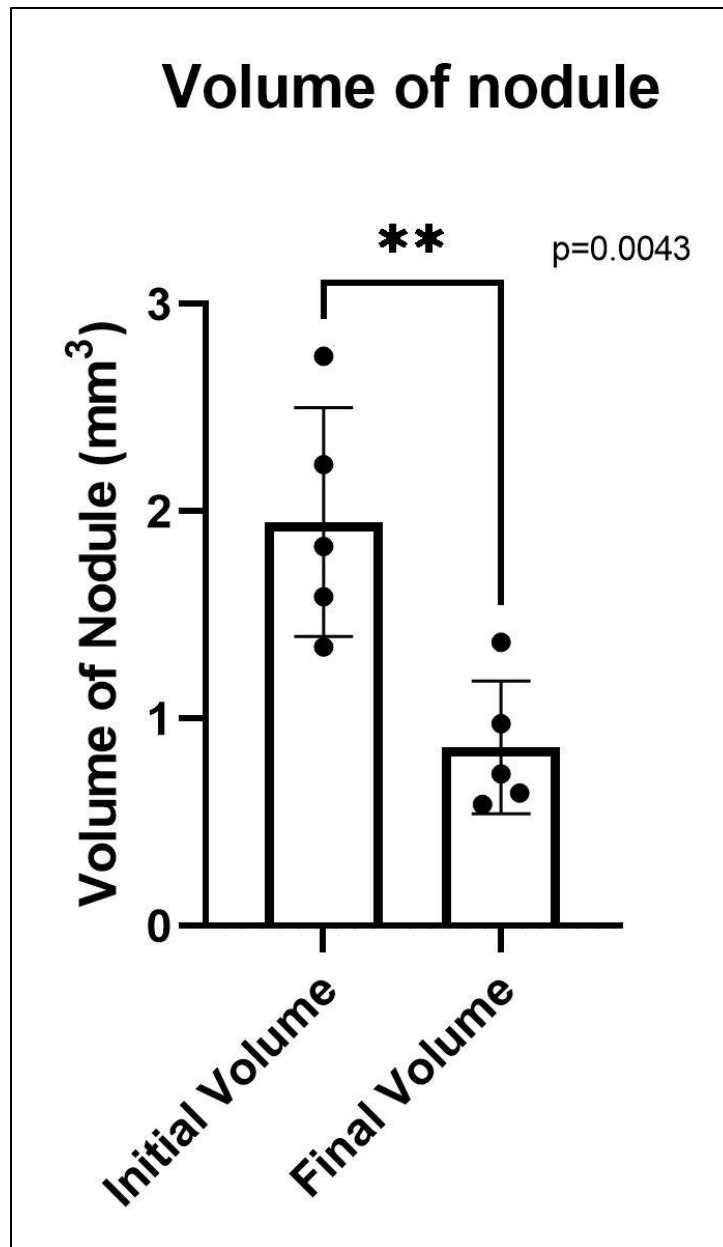


Figure 3.6 Reduction in Volume of Calcific Nodule. This graph depicts the ability of targeted EDTA to reduce the size of the calcific nodules in mice that received at least 5 EDTA treatments (n=5). Each black dot associated with one of the two bars represents the volume of the nodule in an individual mouse. The first bar represents the average volume of nodules before treatment while the second does this but represents average volume of nodules after treatment. Above the graph is a symbol denoting the statistical significance (p=0.0043). Significance was determined using a two-tailed pair t test.

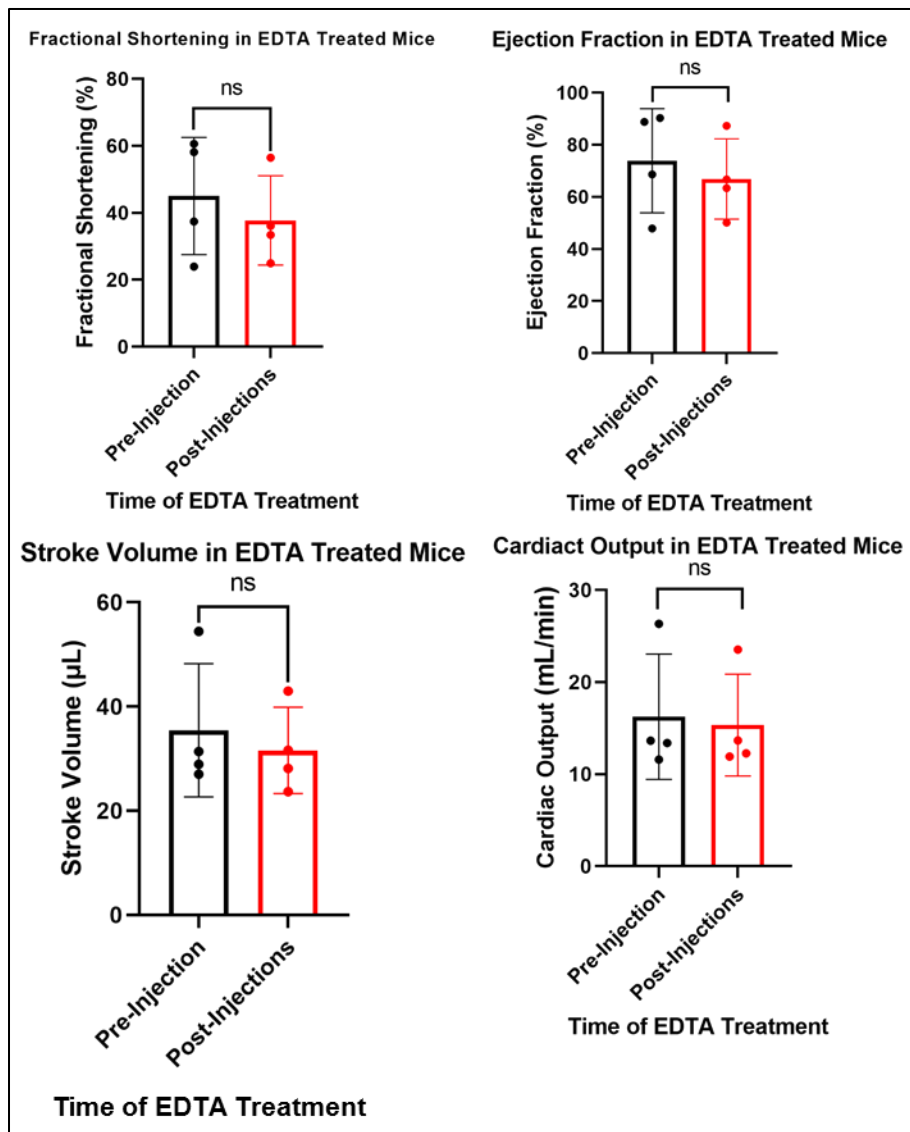


Figure 3.7 Impact of EDTA on Left Ventricular Function. Data on various measurements of LV function of mice that received at least 5 injections of EDTA (n=5) were collected using a Vevo3100 with an MX transducer. The transducer was positioned in the Parasternal short axis view (PSAX) to acquire this data, and the data was processed using VEVO Analysis software provided by the Instrumentation Resource Facility at U of SC School of Medicine-Columbia. The y-axis shows when the data was collected relative to the start of treatment, the x-axis shows the average of the mice at that time relative to treatment. Two-tailed paired t tests indicated that there were no statistically significant changes in any of the LV function measurements over the course of the study.

REFERENCES

- Aikawa E., & Schoen F. J. (2014). “Calcific and degenerative heart valve disease, in Cellular and molecular pathobiology of cardiovascular disease.” Stone J, Homeister JM, Willis MS, editors. Elsevier.; pp. 161–181.
- Akat K., Borggrefe M., & Kaden J. J. (2009). “Aortic valve calcification: basic science to clinical practice.” *Heart.*; 95:616–623.
- Akhurst R. J. (2017). Targeting TGF- β Signaling for Therapeutic Gain. *Cold Spring Harbor perspectives in biology*, 9(10), a022301.
<https://doi.org/10.1101/cshperspect.a022301>
- Bader, J., Carson, M., Enos, R., Velazquez, K., Sougiannis, A., Singh, U., Becker, W., Nagarkatti, M., Fan, D., & Murphy, A. (2020). High-fat diet-fed ovariectomized mice are susceptible to accelerated subcutaneous tumor growth potentially through adipose tissue inflammation, local insulin-like growth factor release, and tumor associated macrophages. *Oncotarget*, 11(49), 4554–4569.
<https://doi.org/10.18632/oncotarget.27832>
- Barnes, P. M., Bloom, B., & Nahin, R. L. (2008). Complementary and alternative medicine use among adults and children: United States, 2007. *National health statistics reports*, (12), 1–23.
- Butcher J.T., & Markwald R.R. (2007). “Valvulogenesis: the moving target.” *Philos Trans R Soc Lond B Biol Sci.*;362:1489–1503.

- Casaclang-Verzosa, G., Enriquez-Sarano, M., Villaraga, H. R., & Miller, J. D. (2017). Echocardiographic Approaches and Protocols for Comprehensive Phenotypic Characterization of Valvular Heart Disease in Mice. *Journal of visualized experiments : JoVE*, (120), 54110. <https://doi.org/10.3791/54110>.
- Charitos, E. I., & Sievers H. H. (2013). “Anatomy of the Aortic Root: Implications for Valve-Sparing Surgery.” *Annals of Cardiothoracic Surgery*, vol., pp. 53–56., <https://doi.org/DOI: 10.3978/j.issn.2225- 319X.2012.11.18>.
- Chen, J. H., Yip, C. Y., Sone, E. D., & Simmons, C. A. (2009). Identification and characterization of aortic valve mesenchymal progenitor cells with robust osteogenic calcification potential. *Am J Pathol*, 174(3), 1109-1119. [doi:10.2353/ajpath.2009.080750](https://doi.org/10.2353/ajpath.2009.080750)
- Chen J. H., & Simmons C. A. (2011). “Cell-matrix interactions in the pathobiology of calcific aortic valve disease: critical roles for matricellular, matricrine, and matrix mechanics cues.” *Circ Res.*; 108:1510–1524.
- Chignalia, A. Z., Oliveira, M. A., Debbas, V., Dull, R. O., Laurindo, F. R., Touyz, R. M., Carvalho, M. H., Fortes, Z. B., & Tostes, R. C. (2015). Testosterone induces leucocyte migration by NADPH oxidase-driven ROS- and COX2-dependent mechanisms. *Clinical science (London, England : 1979)*, 129(1), 39–48. <https://doi.org/10.1042/CS20140548>.
- Chung, C. C., Hsu, R. C., Kao, Y. H., Liou, J. P., Lu, Y. Y., & Chen, Y. J. (2014). Androgen attenuates cardiac fibroblasts activations through modulations of transforming growth factor- β and angiotensin II signaling. *International journal of cardiology*, 176(2), 386–393. <https://doi.org/10.1016/j.ijcard.2014.07.077>

- Clarke, N. E., Clarke, C. N., & Mosher, R. E. (1955). The in vivo dissolution of metastatic calcium; an approach to atherosclerosis. *The American journal of the medical sciences*, 229(2), 142–149. <https://doi.org/10.1097/00000441-195502000-00004>
- Cranton, E. M. (2001). A textbook on EDTA chelation therapy. Hampton Roads Publishing.
- Davison S. L., & Bell R. (2006). Androgen physiology. *Seminars in Reproductive Medicine*. 24(2): 71–7. doi:10.1055/s-2006-939565.
- Derynck R., & Zhang Y. E. (2003). Smad-dependent and Smad-independent pathways in TGF- β family signalling. *Nature* 425: 577–584.
- Donley, G. E., & Fitzpatrick, L. A. (1998). Noncollagenous matrix proteins controlling mineralization; possible role in pathologic calcification of vascular tissue. *Trends in cardiovascular medicine*, 8(5), 199–206. [https://doi.org/10.1016/s1050-1738\(98\)00014-0](https://doi.org/10.1016/s1050-1738(98)00014-0)
- Farzaneh-Far A., Proudfoot D., Shanahan C., & Weissberg P.L. (2001). “Vascular and valvar calcification: recent advances.” *Heart.*; 85:13–17.
- Filip, D. A., Radu, A. & Simionescu, M. (1986). “Interstitial cells of the heart valves possess characteristics similar to smooth muscle cells.” *Circ. Res.* 59, 310–320.
- Goldbarg S. H., Elmariah S., Miller M. A., & Fuster V. (2007). “Insights into degenerative aortic valve disease.” *J Am Coll Cardiol.*; 50:1205–1213.
- Gordon, K. J., & Blobel, G. C. (2008). Role of transforming growth factor- β superfamily signaling pathways in human disease. *Biochim Biophys Acta*, 1782(4), 197-228. doi:10.1016/j.bbadis.2008.01.006

- Heldin, C. H., & Moustakas, A. (2016). Signaling Receptors for TGF- β Family Members. *Cold Spring Harb Perspect Biol*, 8(8). doi:10.1101/cshperspect.a022053
- Heldring, N., Pike, A., Andersson, S., Matthews, J., Cheng, G., Hartman, J., Tujague, M., Ström, A., Treuter, E., Warner, M., & Gustafsson, J. A. (2007). Estrogen receptors: how do they signal and what are their targets. *Physiological reviews*, 87(3), 905–931. <https://doi.org/10.1152/physrev.00026.2006>
- Hinck A. P. (2012). “Structural studies of the TGF- β s and their receptors - insights into evolution of the TGF- β superfamily.” *FEBS letters*, 586(14), 1860–1870. <https://doi.org/10.1016/j.febslet.2012.05.028>
- Ho S. Y. (2009). Structure and anatomy of the aortic root, *European Journal of Echocardiography*, Volume 10, Issue 1, Pages i3–i10
- Huk, D. J., Austin, B. F., Horne, T. E., Hinton, R. B., Ray, W. C., Heistad, D. D., & Lincoln, J. (2016). Valve Endothelial Cell-Derived Tgfb β 1 Signaling Promotes Nuclear Localization of Sox9 in Interstitial Cells Associated With Attenuated Calcification. *Arteriosclerosis, thrombosis, and vascular biology*, 36(2), 328–338. <https://doi.org/10.1161/ATVBAHA.115.306091>
- Ito, I., Hanyu, A., Wayama, M., Goto, N., Katsuno, Y., Kawasaki, S., Nakajima, Y., Kajiro, M., Komatsu, Y., Fujimura, A., Hirota, R., Murayama, A., Kimura, K., Imamura, T., & Yanagisawa, J. (2010). Estrogen inhibits transforming growth factor beta signaling by promoting Smad2/3 degradation. *The Journal of biological chemistry*, 285(19), 14747–14755. <https://doi.org/10.1074/jbc.M109.093039>

- Iung B., Baron G., Butchart E.G., Delahaye F., Gohlke-Bärwolf C., Levang O.W., Tornos P., Vanoverschelde J-L., Vermeer F., & Boersma E. (2003) “A prospective survey of patients with valvular heart disease in Europe: the Euro Heart Survey on Valvular Heart Disease.” *Eur Heart J.*; 24:1231–1243.
- Jian B., Narula N., Li Q. Y., Mohler E. R., III & Levy R. J. (2003). Progression of aortic valve stenosis: TGF-beta1 is present in calcified aortic valve cusps and promotes aortic valve interstitial cell calcification via apoptosis. *Ann Thorac Surg.*; 75:457-465.
- Kaden, J. J., Bickelhaupt, S., Grobholz, R., Vahl, C. F., Hagl, S., Brueckmann, M., Haase, K. K., Dempfle, C. E., & Borggrefe, M. (2004). Expression of bone sialoprotein and bone morphogenetic protein-2 in calcific aortic stenosis. *The Journal of heart valve disease*, 13(4), 560–566.
- Karamched, S. R., Nosoudi, N., Moreland, H. E., Chowdhury, A., & Vyavahare, N. R. (2019). Site-specific chelation therapy with EDTA-loaded albumin nanoparticles reverses arterial calcification in a rat model of chronic kidney disease. *Scientific reports*, 9(1), 2629. <https://doi.org/10.1038/s41598-019-39639-8>
- Kuiper, G. G., Carlsson, B., Grandien, K., Enmark, E., Häggblad, J., Nilsson, S., & Gustafsson, J. A. (1997). Comparison of the ligand binding specificity and transcript tissue distribution of estrogen receptors alpha and b
- Lei, Y., Nosoudi, N., & Vyavahare, N. (2014). Targeted chelation therapy with EDTA-loaded albumin nanoparticles regresses arterial calcification without causing systemic side effects. *Journal of controlled release : official journal of the Controlled Release Society*, 196, 79–86.

- <https://doi.org/10.1016/j.jconrel.2014.09.029> et al. *Endocrinology*, 138(3), 863–870. <https://doi.org/10.1210/endo.138.3.4979>
- Letterio, J. J., & Roberts, A. B. (1998). Regulation of immune responses by TGF-beta. *Annual review of immunology*, 16, 137–161. <https://doi.org/10.1146/annurev.immunol.16.1.137>
- Lindman, B. R., Bonow, R. O., & Otto, C. M. (2013). “Current management of calcific aortic stenosis.” *Circulation research*, 113(2), 223–237. <https://doi.org/10.1161/CIRCRESAHA.111.300084>
- Liu, S., Chen, S., & Zeng, J. (2018). TGF-β signaling: A complex role in tumorigenesis (Review). *Molecular Medicine Reports*, 17, 699-704. <https://doi.org/10.3892/mmr.2017.7970>
- Merryman W. D., Liao J, Parekh A, Candiello J. E., Lin H, & Sacks M. S. (2007) “Differences in tissue-remodeling potential of aortic and pulmonary heart valve interstitial cells.” *Tissue Eng.*;13:2281–2289.
- Messier Jr, R. H., Bass, B. L., Aly, H. M., Jones, J. L., Domkowski, P. W., Wallace, R. B. & Hopkins, R. A. (1994). “Dual structural and functional phenotypes of the porcine aortic valve interstitial population: characteristics of the leaflet myofibroblast”. *J. Surg. Res.* 57, 1–21. (doi:10.1006/ jsre.1994.1102)
- Miller, J. D., Chu, Y., Brooks, R. M., Richenbacher, W. E., Peña-Silva, R., & Heistad, D. D. (2008). Dysregulation of antioxidant mechanisms contributes to increased oxidative stress in calcific aortic valvular stenosis in humans. *Journal of the American College of Cardiology*, 52(10), 843–850. <https://doi.org/10.1016/j.jacc.2008.05.043>

- Miller, J. D., Weiss, R. M., & Heistad, D. D. (2011). Calcific aortic valve stenosis: methods, models, and mechanisms. *Circulation research*, 108(11), 1392–1412.
<https://doi.org/10.1161/CIRCRESAHA.110.234138>.
- Misfeld, M., & Sievers, H. H. (2007). Heart valve macro- and microstructure. *Philosophical transactions of the Royal Society of London. Series B, Biological sciences*, 362(1484), 1421–1436.
<https://doi.org/10.1098/rstb.2007.2125>
- Mohler, E.R. III. (2004). “Mechanisms of aortic valve calcification.” *Am J Cardiol.*; 94:1396–1402, A1396.
- Molin, D. G., Bartram, U., Van der Heiden, K., Van Iperen, L., Speer, C. P., Hierck, B. P., & Gittenberger-de-Groot, A. C. (2003). “Expression patterns of Tgfbeta1-3 associate with myocardialisation of the outflow tract and the development of the epicardium and the fibrous heart skeleton.” *Dev Dyn*, 227(3), 431-444.
doi:10.1002/dvdy.10314
- Morikawa, M., Derynck, R., & Miyazono, K. (2016). TGF- β and the TGF- β Family: Context-Dependent Roles in Cell and Tissue Physiology. *Cold Spring Harbor perspectives in biology*, 8(5), a021873.
<https://doi.org/10.1101/cshperspect.a021873>
- Morikawa, M., Koinuma, D., Miyazono, K., & Heldin, C. H. (2013). Genome-wide mechanisms of Smad binding. *Oncogene*, 32(13), 1609-1615.
doi:10.1038/onc.2012.191
- Nishimura, R. A., Otto, C. M., Bonow, R. O., Carabello, B. A., Erwin, J. P., 3rd, Guyton, R. A., O’Gara, P. T., Ruiz, C. E., Skubas, N. J., Sorajja, P., Sundt, T. M., 3rd,

- Thomas, J. D., & ACC/AHA Task Force Members (2014). 2014 AHA/ACC “Guideline for the Management of Patients With Valvular Heart Disease: executive summary: a report of the American College of Cardiology/American Heart Association Task Force on Practice Guidelines.” *Circulation*, 129(23), 2440–2492. <https://doi.org/10.1161/CIR.0000000000000029>.
- Nosoudi, N., Chowdhury, A., Siclari, S., Karamched, S., Parasaram, V., Parrish, J., Gerard, P., & Vyavahare, N. (2016). Reversal of Vascular Calcification and Aneurysms in a Rat Model Using Dual Targeted Therapy with EDTA- and PGG-Loaded Nanoparticles. *Theranostics*, 6(11), 1975–1987. <https://doi.org/10.7150/thno.16547>
- Nosoudi, N., Nahar-Gohad, P., Sinha, A., Chowdhury, A., Gerard, P., Carsten, C. G., Gray, B. H., & Vyavahare, N. R. (2015). Prevention of abdominal aortic aneurysm progression by targeted inhibition of matrix metalloproteinase activity with batimastat-loaded nanoparticles. *Circulation research*, 117(11), e80–e89. <https://doi.org/10.1161/CIRCRESAHA.115.307207>
- O’Brien KD. (2007). “Epidemiology and genetics of calcific aortic valve disease.” *J Investig Med.*; 55:284–291.
- O’Kane, S., & Ferguson, M. W. (1997). Transforming growth factor beta s and wound healing. *The international journal of biochemistry & cell biology*, 29(1), 63–78. [https://doi.org/10.1016/s1357-2725\(96\)00120-3](https://doi.org/10.1016/s1357-2725(96)00120-3)
- Pai, A. S., & Giachelli, C. M. (2010). Matrix remodeling in vascular calcification associated with chronic kidney disease. *Journal of the American Society of*

- Nephrology : JASN*, 21(10), 1637–1640.
<https://doi.org/10.1681/ASN.2010040349>
- Pitt, C. G., Gratzl, M. M., Kimmel, G. L., Surles, J., & Schindler, A. (1981). Aliphatic polyesters II. The degradation of poly (DL-lactide), poly (epsilon-caprolactone), and their copolymers in vivo. *Biomaterials*, 2(4), 215–220.
[https://doi.org/10.1016/0142-9612\(81\)90060-0](https://doi.org/10.1016/0142-9612(81)90060-0)
- Pomerance A. (1967). “Ageing changes in human heart valves.” *Br Heart J.*; 29:222–231.
- Prossnitz, E. R., Arterburn, J. B., Smith, H. O., Oprea, T. I., Sklar, L. A., & Hathaway, H. J. (2008). Estrogen signaling through the transmembrane G protein-coupled receptor GPR30. *Annual review of physiology*, 70, 165–190.
<https://doi.org/10.1146/annurev.physiol.70.113006.100518>
- Rajamannan N. M., Evans F. J., Aikawa E., Grande-Allen K. J., Demer L. L., Heistad D. D., Simmons C. A., Masters K. S., Mathieu P., O'Brien K. D., Schoen F. J., Towler D. A., Yoganathan A. P., & Otto C. M. (2011). “Calcific aortic valve disease: not simply a degenerative process: A review and agenda for research from the National Heart and Lung and Blood Institute Aortic Stenosis Working Group.” Executive summary: Calcific aortic valve disease-update. *Circulation*. 2011;124:1783-1791.
- Richards, J., El-Hamamsy, I., Chen, S., Sarang, Z., Sarathchandra, P., Yacoub, M. H., Chester, A. H., & Butcher, J. T. (2013). Side-specific endothelial-dependent regulation of aortic valve calcification: interplay of hemodynamics and nitric

- oxide signaling. *The American journal of pathology*, 182(5), 1922–1931.
<https://doi.org/10.1016/j.ajpath.2013.01.037>
- Robertson, I. B., & Rifkin, D. B. (2016). Regulation of the Bioavailability of TGF- β and TGF- β -Related Proteins. *Cold Spring Harb Perspect Biol.*, 8(6).
doi:10.1101/cshperspect.a021907
- Rosenbloom, J., Abrams, W. R., & Mecham, R. (1993). Extracellular matrix 4: the elastic fiber. *FASEB journal : official publication of the Federation of American Societies for Experimental Biology*, 7(13), 1208–1218.
- Rutkovskiy A., Malashicheva A., Sullivan G., Bogdanova M., Kostareva A., Stensl kken K. O., Fiane A., & Vaage J. (2017) “Valve Interstitial Cells: The Key to Understanding the Pathophysiology of Heart Valve Calcification.” *J Am Heart Assoc.*;6(9):e006339. doi: 10.1161/JAHA.117.006339. PMID: 28912209; PMCID: PMC5634284.
- Sahoo, S., Meijles, D. N., & Pagano, P. J. (2016). NADPH oxidases: key modulators in aging and age-related cardiovascular diseases?. *Clinical science (London, England : 1979)*, 130(5), 317–335. <https://doi.org/10.1042/CS20150087>
- Sakai, L. Y., Keene, D. R., & Engvall, E. (1986). Fibrillin, a new 350-kD glycoprotein, is a component of extracellular microfibrils. *The Journal of cell biology*, 103(6 Pt 1), 2499–2509. <https://doi.org/10.1083/jcb.103.6.2499>
- Seely, D. M., Wu, P., & Mills, E. J. (2005). EDTA chelation therapy for cardiovascular disease: a systematic review. *BMC cardiovascular disorders*, 5, 32.
<https://doi.org/10.1186/1471-2261-5-32>.

- Seya, K., Yu, Z., Kanemaru, K., Daitoku, K., Akemoto, Y., Shibuya, H., Fukuda, I., Okumura, K., Motomura, S., & Furukawa, K. (2011). Contribution of bone morphogenetic protein-2 to aortic valve calcification in aged rat. *Journal of pharmacological sciences*, 115(1), 8–14. <https://doi.org/10.1254/jphs.10198fp>
- Shi Y., & Massague´ J. 2003. Mechanisms of TGF-b signaling from cell membrane to the nucleus. *Cell* 113: 685–700.
- Sievers, H. H., & Schmidtke C.A. (2007). Classification system for the bicuspid aortic valve from 304 surgical specimens. *J Thorac Cardiovasc Surg*; 133:1226-33.
- Sinha, A., Shaporev, A., Nosoudi, N., Lei, Y., Vertegel, A., Lessner, S., & Vyavahare, N. (2014). Nanoparticle targeting to diseased vasculature for imaging and therapy. *Nanomedicine : nanotechnology, biology, and medicine*, 10(5), 1003–1012. <https://doi.org/10.1016/j.nano.2014.02.002>
- Taylor, P. M., Batten, P., Brand, N. J., Thomas, P. S., & Yacoub, M. H. (2003). “The cardiac valve interstitial cell.” *Int J Biochem Cell Biol*, 35(2), 113-118.
- Thubrikar, MJ. (1981). *The Aortic Valve*. 1st ed. Boca Raton, Florida, US: CRC Press, Inc.,
- Tuck, S., & Francis, R. (2009). Testosterone, bone and osteoporosis. *Frontiers of hormone research*, 37, 123–132. <https://doi.org/10.1159/000176049>
- Ueda K., Adachi Y., Liu P., Fukuma N., & Takimoto E. (2019). Regulatory Actions of Estrogen Receptor Signaling in the Cardiovascular System. *Front Endocrinol (Lausanne)*; doi:10:909
- Visconti, R. P., Ebihara, Y., LaRue, A. C., Fleming, P. A., McQuinn, T. C., Masuya, M., & Drake, C. J. (2006). “An in vivo analysis of hematopoietic stem cell potential:

- hematopoietic origin of cardiac valve interstitial cells.” *Circ Res*, 98(5), 690-696.
doi:10.1161/01.RES.0000207384.81818.d4
- Weinhaus, A. J. (2015). Anatomy of the Human Heart. In: Iaizzo P. (eds) Handbook of Cardiac Anatomy, Physiology, and Devices. Springer, Cham.
- Wu, L., Wu, Y., Gathings, B., Wan, M., Li, X., Grizzle, W., Liu, Z., Lu, C., Mao, Z., & Cao, X. (2003). Smad4 as a transcription corepressor for estrogen receptor alpha. *The Journal of biological chemistry*, 278(17), 15192–15200.
<https://doi.org/10.1074/jbc.M212332200>
- Xu S., Liu A. C., & Gotlieb A.I. (2010). “Common pathogenic features of atherosclerosis and calcific aortic stenosis: role of transforming growth factor-b.” *Cardiovasc Pathol.*; 19:236–247.
- Yutzey K. E., Demer L. L., Body S. C., Huggins G. S., Towler D. A., Giachelli C. M., Hofmann-Bowman M. A., Mortlock D. P., Rogers M. B., Sadeghi M. M., & Aikawa E. (2014) “Calcific aortic valve disease: a consensus summary from the Alliance of Investigators on Calcific Aortic Valve Disease.” *Arterioscler Thromb Vasc Biol.*; 34:2387-93.
- Zapata, E., Ventura, J. L., De la Cruz, K., Rodriguez, E., Damián, P., Massó, F., Montaña, L. F., & López-Marure, R. (2005). Dehydroepiandrosterone inhibits the proliferation of human umbilical vein endothelial cells by enhancing the expression of p53 and p21, restricting the phosphorylation of retinoblastoma protein, and is androgen- and estrogen-receptor independent. *The FEBS journal*, 272(6), 1343–1353. <https://doi.org/10.1111/j.1742-4658.2005.04563.x>

- Zhao, B., & Chen, Y. G. (2014). Regulation of TGF- β Signal Transduction. *Scientifica*; 874065. <https://doi.org/10.1155/2014/874065>
- Zhang, B., Miller, V. M., & Miller, J. D. (2019). Influences of Sex and Estrogen in Arterial and Valvular Calcification. *Frontiers in endocrinology*, 10, 622. <https://doi.org/10.3389/fendo.2019.00622>
- Zhang, Y. E. (2009). Non-Smad pathways in TGF-beta signaling. *Cell Res.*, 19(1), 128-139. doi:10.1038/cr.2008.328
- Zhou, S., Turgeman, G., Harris, S. E., Leitman, D. C., Komm, B. S., Bodine, P. V., & Gazit, D. (2003). Estrogens activate bone morphogenetic protein-2 gene transcription in mouse mesenchymal stem cells. *Molecular endocrinology (Baltimore, Md.)*, 17(1), 56–66. <https://doi.org/10.1210/me.2002-0210>

APPENDIX A: SUPPLEMENTARY FIGURE

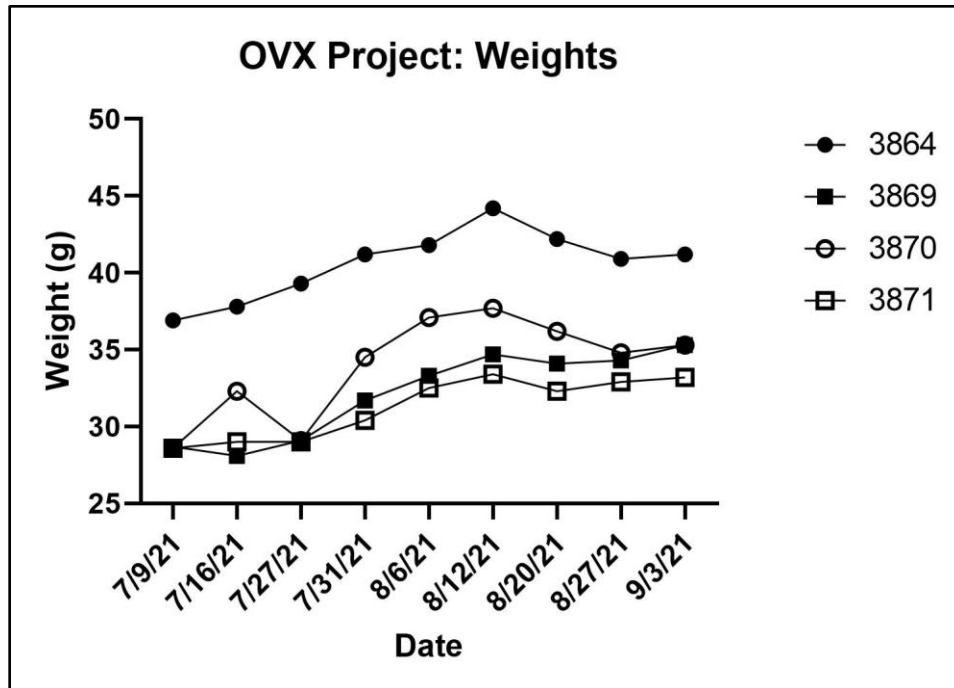


Figure A. 1 Weights of Mice in Preliminary OVX Study. This graph tracks the weights of the four mice on a high fat diet over the course of the preliminary OVX study. The y-axis shows the date the measurement was recorded, while the x-axis shows the weight in grams. There is a legend on the right-hand side of the graph showing which mouse is associated with the data plotted.

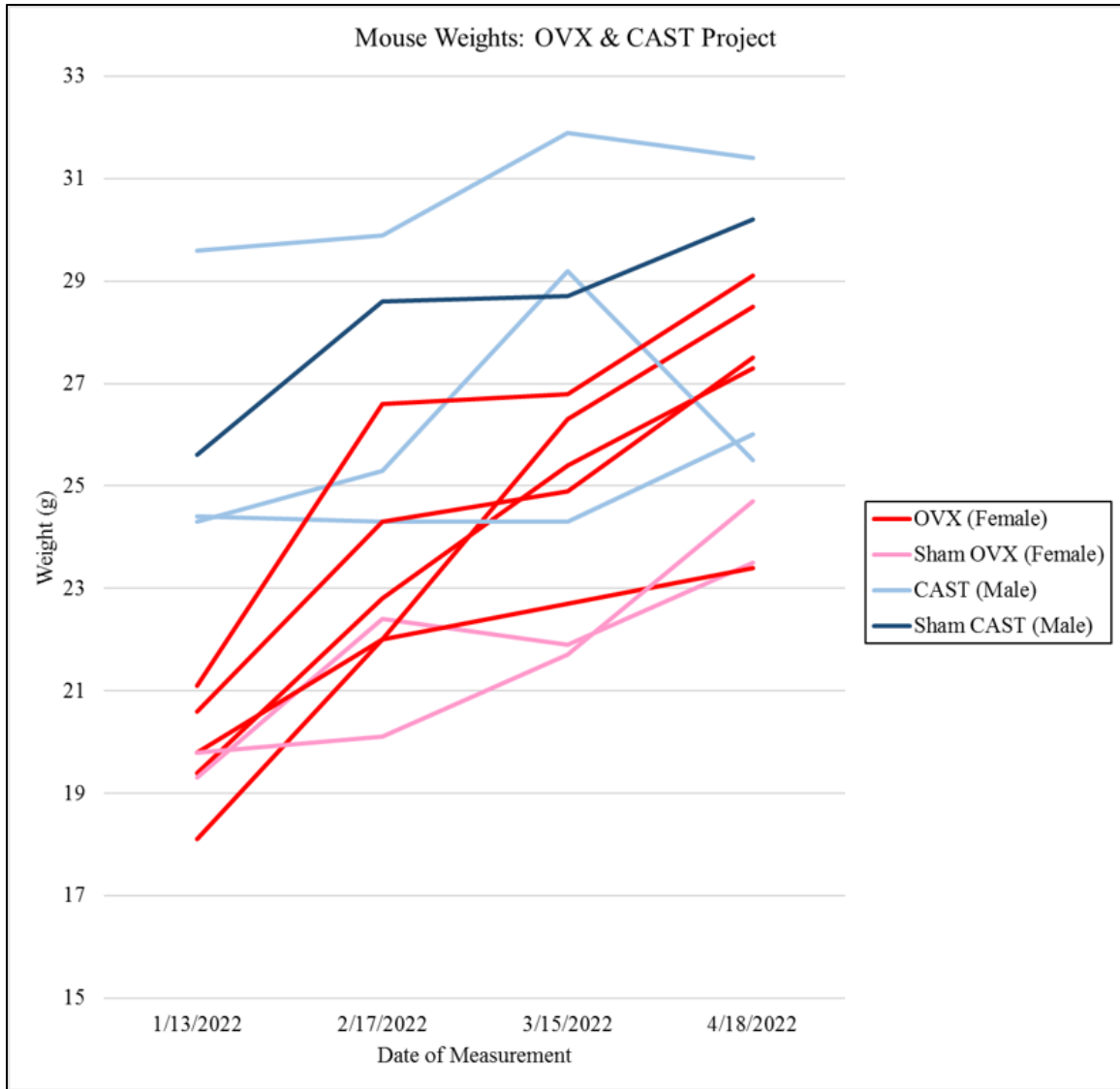


Figure A. 2 Weights of Mice in OVX and CAST Study. This graph tracks the weights of the mice (n=11) on a normal chow diet over the course of the OVX & CAST study. The y-axis shows the date the measurement was recorded, while the x-axis shows the weight in grams. There is a legend on the right-hand side of the graph showing which mouse is associated with the data plotted.

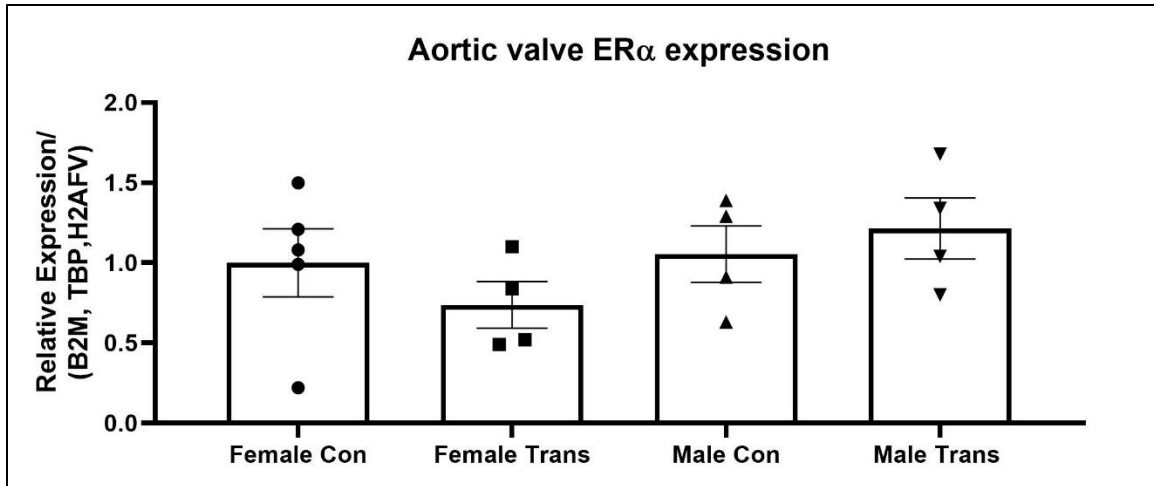


Figure A. 3 qPCR Comparison of ER α Expression in AV of Mice. This graph shows a comparison of ER α expression in the AV of male and female control and transgenic mice. None of the values are significantly different from the others. This image comes from a qPCR done by Dr. Enos' lab.